THE ASTROPHYSICAL JOURNAL, 539:815–833, 2000 August 20

AN *IUE* ATLAS OF PRE–MAIN-SEQUENCE STARS. II. FAR-ULTRAVIOLET ACCRETION DIAGNOSTICS IN T TAURI STARS

CHRISTOPHER M. JOHNS-KRULL,[1] JEFF A. VALENTI,[2] AND JEFFREY L. LINSKY
JILA, University of Colorado and NIST, Campus Box 440, Boulder, CO 80309; cmj@ssl.berkeley.edu, valenti@stsci.edu, jlinsky@jila.colorado.edu
Received 1999 November 5; accepted 2000 March 9

ABSTRACT

We use our ultraviolet (UV) atlas of pre–main-sequence stars constructed from all useful, short-wavelength, low-resolution spectra in the *International Ultraviolet Explorer* (*IUE*) satellite Final Archive to analyze the short-wavelength UV properties of 49 T Tauri stars (TTSs). We compare the line and continuum fluxes in these TTSs with each other and with previously published parameters of these systems, including rotation rate, infrared excess, and mass accretion rate. The short-wavelength continuum in the classical TTSs (CTTSs) appears to originate in a ∼10,000 K optically thick plasma, while in the naked TTSs (NTTSs—stars without dusty disks) the continuum appears to originate in the stellar atmosphere. We show that all of the TTSs in our sample lie in the regime of "saturated" magnetic activity due to their small Rossby numbers. However, while some of the TTSs show emission line surface fluxes consistent with this saturation level, many CTTSs show significantly stronger emission than predicted by saturation. In these stars, the emission line luminosity in the high ionization lines present in the spectrum between 1200 and 2000 Å correlates well with the mass accretion rate. Therefore, we conclude that the bulk of the short-wavelength emission seen in CTTSs results from accretion related processes and not from dynamo-driven magnetic activity. Using CTTSs with known mass accretion rates, we calibrate the relationship between $\dot{M}$ and $L_{\rm C\,IV}$ to derive the mass accretion rate for some CTTSs which for various reasons have never had their mass accretion rates measured. Finally, several of the CTTSs show strong emission from molecular hydrogen. While emission from H_2 cannot form in gas at a temperature of $\sim 10^5$ K, the strength of the molecular hydrogen emission is nevertheless well correlated with all the other emissions displayed in the *IUE* short-wavelength bandpass. This suggests that the H_2 emission is in fact fluorescent emission pumped by the emission (likely Lyα) from hotter gas.

Subject headings: accretion, accretion disks — circumstellar matter — stars: activity — stars: pre–main-sequence

1. INTRODUCTION

T Tauri stars (TTSs) were originally defined as a class due to their spectral peculiarities (Herbig 1962). These include emission (sometimes quite strong) in traditional chromospheric diagnostics such as Hα, Ca II H and K, and the Ca II infrared (IR) triplet. Association with nebular material, their placement in the HR diagram, and the presence of the Li I 6707 Å resonance line indicates youth in TTSs. The general similarity of low-resolution spectra of TTSs to the spectra of flare stars and other active late-type stars led to the proposal that TTSs were just very active (perhaps due to their youth) versions of these objects (Herbig 1970). The source of this activity was assumed to be the same sort of magnetic dynamo which appears to be active in main-sequence stars.

The notion that TTSs were very magnetically active stars led to the development of a number of "deep chromosphere" models to try and explain their optical spectrum (Cram 1979; Herbig & Soderblom 1980; Cram, Giampapa, & Imhoff 1980; Giampapa et al. 1981; Calvet, Basri, & Kuhi 1984). Observations of TTSs with the *International Ultraviolet Explorer* (*IUE*) satellite detected hot transition region lines (such as Si IV and C IV), and these observations appeared to support the deep chromosphere model (e.g., Cram et al. 1980). Some investigators also recognized the need for an overlying wind (e.g., Brown, de M. Ferraz, & Jordan 1984). Observations of the far-UV line fluxes in TTSs were combined with those of main-sequence stars to help derive activity and magnetic spin-down relationships (Hartmann et al. 1984; Barry, Hege, & Cromwell 1984; Simon, Herbig, & Boesgaard 1985). A good summary of the *IUE* observations of TTSs and their interpretation in terms of chromospheric activity and winds can be found in Imhoff & Appenzeller (1987).

While the deep chromosphere models were somewhat successful at explaining the appearance of TTS spectra, these models began to have some problems as more and different observational data became available. High-resolution spectra of Hα and the Ca II H and K lines (and Mg II *h* and *k* from *IUE* in the UV) showed that these lines were much broader than typically seen in active main-sequence stars. These observations also showed the presence of the wind, and models started to include a wind on top of the deep chromosphere models to try to reconcile the situation (Brown et al. 1984). It seemed somewhat natural that the energy source required to drive the strong winds of TTSs would also produce a deep chromosphere. Calvet et al. (1984) demonstrated that a single component, plane parallel, static chromosphere is unable to simultaneously explain the observed fluxes of the Ca II and Mg II resonance lines, and the levels of Balmer line and continuum emission. Instead, these authors proposed a circumstellar region of significant geometrical extent to explain the observed blue

[1] Now at Space Sciences Laboratory, University of California, Berkeley, CA 94720.
[2] Now at Space Telescope Science Institute, 3700 San Martin Drive, Baltimore, MD 21218.

excess emission (veiling) and the total fluxes in the Balmer lines.

During this time, evidence for accretion onto TTSs began to accumulate. Lynden-Bell & Pringle (1974) were the first to suggest that the combination of a viscous accretion disk and a surface boundary layer might account for the excess continuum emission of many TTSs; however, this suggestion went largely unheeded for some time. Starting in the late 1980s, many different lines of evidence showed that the classical TTSs (CTTSs) are surrounded by active accretion disks and that disk material is accreting onto the surface of the star (see reviews by Bertout 1989; Basri & Bertout 1993). The naked TTSs (NTTSs) are comparably young stars (as indicated by their placement in the HR diagram and the presence of strong Li I absorption in their spectra) without accretion disks (Walter 1987). The NTTSs appear to derive their activity entirely from a magnetic dynamo active in these relatively rapidly rotating, young stars (e.g., Bouvier 1990; Walter & Byrne 1998). The term weak TTS (WTTS) is also often used to refer to diskless TTSs, but this term can be confusing: WTTS is a definition based solely on the equivalent width of the Hα emission line. For intrinsically brighter (usually earlier spectral type) TTSs, the Hα equivalent width can be small enough to earn the label WTTS despite the very definite presence of an accretion disk. On the other hand, though CTTS is also strictly speaking a definition based on equivalent width, all known CTTSs also exhibit evidence for active accretion from a circumstellar accretion disk (with the one possible exception of CS Cha, which we discuss further below). Therefore, we will use CTTS to refer to those stars with disks and NTTS to refer to diskless TTSs.

While this accretion model for CTTSs has been very successful at explaining a wide variety of the observational peculiarities in these objects, relatively little work has been done to see to what degree the *IUE* observations fit into or elucidate this paradigm. CTTSs are known to display both periodic and aperiodic photometric variations. Spot modeling of multicolor photometry in CTTSs indicates the presence of large dark spots on these stars (traditional "starspots") as well as regions of the photosphere with substantially higher temperature than the majority of the surface (e.g., Bouvier, Bertout, & Bouchet 1986; Bertout, Basri, & Bouvier 1988; Bouvier & Bertout 1989; Bouvier et al. 1993; Bouvier et al. 1995). Spectroscopic evidence in the form of the filling in of photospheric lines by a continuum "veiling" source has also been found indicating "hot-spots" on the surfaces of CTTSs (Basri & Batalha 1990; Hartmann & Kenyon 1990; Hartigan et al. 1991; Valenti, Basri, & Johns 1993a; Gullbring et al. 1998). It is believed that these "hot-spots" are produced by the accretion of material from the circumstellar disk onto the surface of the star.

Originally, this accretion onto the star was thought to occur through an equatorial boundary layer which was assumed to be axisymmetric. (Lynden-Bell & Pringle 1974). This interpretation has largely been replaced by the concept of magnetospheric accretion in which the stellar magnetic field truncates the accretion disk at some distance from the star and material flows along the field lines to the stellar surface preferentially at high latitude (Uchida & Shibata 1984; Bertout et al. 1988; Camenzind 1990; Königl 1991; Shu et al. 1994; Paatz & Camenzind 1996). When the accreting disk material strikes the stellar surface, it presumably shocks, creating a hot accretion spot which is responsible for much of the optical excess emission seen in CTTSs. While this magnetospheric accretion paradigm has become quite popular in the star formation community, relatively little work has been done to revisit the extensive *IUE* observations of TTSs to see how they fit into the current model. Simon, Vrba, & Herbst (1990) present simultaneous *IUE* spectra and optical photometry of the CTTS BP Tau, showing that the UV continuum and emission lines in this star vary in phase with the optical excess emission. Simon, Vrba, & Herbst 1990 interpret these results in terms of the magnetospheric accretion model of Uchida & Shibata (1984). Similar results and interpretation were given for the CTTS DI Cep by Gómez de Castro & Fernández (1996). Gómez de Castro & Franqueira (1997) repeated the monitoring campaign on the CTTS BP Tau, noting differences in the temporal behavior of the O I and He II lines compared to lines such as C IV, Si II, and Mg II, but again concluding these results were consistent with the magnetospheric accretion paradigm.

Along with this recent observational work, theoretical investigations have begun into the structure of the accretion shock in the magnetospheric accretion model. Lamzin (1995, 1998) has made some tentative calculations of the structure of the accretion shock aimed at explaining the continuum and narrow emission line components seen in CTTSs. Calvet et al. (1996) made initial calculations of C IV line profiles expected from magnetospheric accretion flows and the resulting shocks at the stellar surface for comparison with high-resolution line profiles observed with *HST* (Valenti et al. 1993b). However, Calvet et al. (1996) did not allow for a contribution from the stellar transition region, and the temperature structure in these models had to be assumed. More recently, Calvet & Gullbring (1998) have made detailed calculations of the structure of the accretion shock on CTTSs, predicting the emergent optical spectrum and finding good agreement with the observations. Gómez de Castro & Lamzin (1999) have applied the models of Lamzin (1995, 1998) and find that they produce UV emission lines comparable in strength to those observed in a handful of CTTSs. On the other hand, CTTSs are known to possess strong, extensive magnetic fields (Johns-Krull & Valenti 2000), and no systematic study has been done to see to what extent the *IUE* emissions of TTSs result from magnetic related processes or accretion related processes. The recent completion of the *IUE* Final Archive and compilation of an *IUE* atlas of pre–main-sequence stars (Valenti, Johns-Krull, & Linsky 2000, hereafter Paper I) offer an excellent database to pursue such a study.

2. OBSERVATIONS

2.1. *The Pre–Main-Sequence Stars SWP Atlas*

All of the *IUE* observations of TTSs discussed in this work come from the short-wavelength pre–main-sequence *IUE* atlas described in Paper I. The fluxes used for this investigation come directly from Table 5 of that paper. Briefly, these fluxes were measured for each TTS, using a weighted mean spectrum constructed from all available *IUE* low-dispersion spectra. It is important to note that the spectra presented in Paper I come from the *IUE* Final Archive (Nichols & Linsky 1996) and therefore are relatively free from the fixed-pattern noise present in the old IUESIPS reductions. Not only does this result in an increase in signal-to-noise for each individual spectrum, but it also allows us to sum spectra and improve the signal-to-noise at nearly the Poisson rate. We refer the reader to Paper I for further details on the construction of the atlas and measurements of the various fluxes. The fluxes tabulated in Paper I are mean continuum fluxes at 1750 and 1958 Å, as well as the integrated line fluxes of several features including lines of N v, Si iv, C iv, H_2, and others.

2.2. *System Parameters from the Literature*

One of the main goals of this work is to compare *IUE* short-wavelength emission to various stellar and system parameters, such as rotation rate, IR excess, and mass accretion rate. We therefore combed the literature for estimates of these various parameters for the TTSs in our *IUE* atlas. These values are listed in Table 1 along with references to where the individual estimates came from. There are sometimes numerous estimates for particular quantities for any given TTS, and they do not always agree. In compiling the numbers in Table 1, we gave preference to more recent estimates and those presented in large studies of several stars, hoping to achieve a more uniform sample of values. While individual estimates may not be totally accurate, we use these data in statistical comparisons with the *IUE* data and look only for general trends. Uncertainties in the derived UV fluxes and luminosities as a result of uncertainties in the extinction are the largest source of error in this analysis. Typical variations in the derived extinction values can produce a factor of 2 change in the derived flux or luminosity. However, these UV emission quantities typi-

TABLE 1

TTS Stellar Data from the Literature

Index	Star	Spectral Type	Class	T_{eff} (K)	A_V (mag)	M_* ($M_\odot$)	R_* ($R_\odot$)	L_* ($L_\odot$)	Distance (pc)	P_{rot} (days)	$v \sin i$ (km s^{-1})	τ_c (days)	$\dot{M}$ ($M_\odot$ yr^{-1})	$\Delta(H-K)$ (mag)
3	LkHα 264	K5[a]	CTTS	4395[b]	0.70[c]	...	1.2[c]	...	...	...	...	...	...	...
4	HH 12/107	M0[a]	CTTS	3802[b]	...	...	...	...	...	...	...	...	...	...
6	Tap 17	F8[d]	NTTS	6115[e]	0.10[d]	1.3[d]	1.4[d]	2.9[d]	140[f]	...	25[d]	181[g]	...	0.0[h]
8	V410 Tau	K7[i]	NTTS	4973	0.00[i]	1.5[j]	2.6[j]	1.9[i]	140[f]	1.9[k]	65[l]	99[g]	...	0.1[h]
9	BP Tau	K7[f]	CTTS	3999[f]	0.51[m]	0.5[m]	2.0[m]	0.9[m]	140[f]	7.6[j]	<10[l]	221[n]	1.6(−7)[f]	0.2[h]
10	DE Tau	M1.5[f]	CTTS	3573[f]	0.62[m]	0.3[m]	2.5[m]	0.9[m]	140[f]	7.6[o]	<10[l]	163[n]	3.2(−7)[f]	0.2[h]
11	RY Tau	K1[f]	CTTS	5082[f]	0.29[p]	1.6[f]	2.4[f]	3.5[f]	140[f]	5.6[k]	52[q]	130[n]	2.5(−8)[f]	0.9[h]
12	HD 283572	G5[i]	NTTS	5522	0.57[i]	2.0[d]	2.9[d]	6.9[d]	140[f]	1.6[j]	80[q]	75[g]	...	0.0[h]
13	T Tau	K0[r]	CTTS	5199	1.00[r]	2.0[r]	3.4[r]	7.5[r]	140[f]	2.8[k]	20[l]	142[g]	...	0.6[h]
14	DF Tau	M2[f]	CTTS	3499[f]	0.45[m]	0.3[m]	3.4[m]	2.0[m]	140[f]	8.5[j]	20[l]	146[n]	1.3(−6)[f]	0.3[h]
15	DG Tau	K5[f]	CTTS	4395[f]	1.66[p]	0.7[f]	2.3[f]	1.7[f]	140[f]	6.3[o]	20[l]	226[n]	2.0(−6)[f]	0.7[h]
17	UX Tau A	K2[s]	NTTS	4898[s]	0.20[s]	1.1[s]	1.4[s]	1.0[s]	140[f]	2.7[j]	20[l]	82[g]	...	...
18	DK Tau	K7[f]	CTTS	3999[f]	1.42[m]	0.4[m]	2.5[m]	1.5[m]	140[f]	8.4[o]	12[l]	188[n]	4.0(−7)[f]	0.5[h]
19	L1551/IRS5	K2[t]	CTTS	4898[b]	...	...	...	...	140	...	...	...	...	...
22	GI Tau	M0[f]	CTTS	3802[f]	1.34[m]	0.7[m]	1.7[m]	0.9[m]	140[f]	7.2[u]	12[v]	188[n]	1.3(−7)[f]	0.4[h]
24	DL Tau	M0[f]	CTTS	3802[f]	0.88[p]	0.4[f]	1.9[f]	0.7[f]	140[f]	...	<10[l]	216[n]	2.0(−7)[f]	0.4[h]
25	AA Tau	M0[f]	CTTS	3802[f]	0.74[m]	0.5[m]	1.7[m]	0.7[m]	140[f]	8.2[j]	10[l]	231[n]	1.3(−7)[f]	0.2[h]
27	DR Tau	K7[f]	CTTS	3999[f]	1.66[p]	0.4[f]	2.7[f]	1.7[f]	140[f]	...	<10[l]	192[n]	7.9(−6)[f]	0.6[h]
28	DS Tau	K2[f]	CTTS	4898[f]	0.34[m]	0.9[m]	1.4[m]	0.6[m]	140[f]	...	<10[l]	110[n]	2.5(−7)[f]	0.3[h]
29	GM Aur	K7[f]	CTTS	3999[f]	0.31[m]	0.5[m]	1.8[m]	0.7[m]	140[f]	12.0[o]	13[l]	197[n]	2.5(−8)[f]	0.1[h]
30	Lk Ca 19	K5[d]	NTTS	4395[d]	0.00[d]	1.2[d]	1.7[d]	1.6[d]	140[f]	2.2[o]	21[d]	127[g]	...	...
32	SU Aur	G2[r]	CTTS	5767[s]	0.93[r]	2.0[r]	3.1[r]	9.6[r]	140[f]	3.0[w]	60[q]	47[g]	...	0.4[h]
35	RW Aur A	K4[f]	CTTS	4592[f]	1.14[p]	0.9[f]	2.4[f]	2.3[f]	140[f]	5.4[j]	15[l]	218[n]	1.6(−6)[f]	0.5[h]
38	GW Ori	G5[j]	CTTS	5670	0.82[j]	3.1[j]	8.5[j]	66.1[j]	460[x]	3.3[j]	40[v]	...	...	...
42	λ Ori X1	K1[y]	NTTS	5082[b]	...	...	...	...	500[y]	...	...	...	...	...
64	HBC 167	G5[z]		5780[z]	...	...	...	...	...	...	19[z]	...	...	...
93	TW Hya	K7[a]	CTTS	3999[b]	...	...	...	...	...	...	...	...	...	...
95	CS Cha	K5[z]	CTTS	4395[z]	0.85[aa]	1.7[bb]	2.6[cc]	2.7[aa]	215[aa]	...	21[z]	231[g]	...	0.0[dd]
98	VW Cha	K5[ee]	CTTS	4395[ff]	2.39[aa]	1.4[bb]	3.6[cc]	4.2[aa]	215[aa]	...	26[j]	236[g]	...	0.4[dd]
102	Sz 41	K0[z]	CTTS	5199[z]	1.17[aa]	1.6[bb]	2.5[cc]	2.8[aa]	215[aa]	...	38[z]	206[g]	...	0.3[dd]
103	CV Cha	G8[aa]	CTTS	5451[aa]	1.67[aa]	2.1[bb]	3.2[aa]	8.0[aa]	215[aa]	4.4[j]	32[z]	78[g]	...	0.4[dd]
112	Sco PMS 005	G2[gg]	NTTS	5819[e]	0.20[gg]	2.1[gg]	2.6[cc]	6.8[gg]	160[gg]	...	57[gg]	12[g]	...	0.0[hh]
113	RU Lup	K7[ee]	CTTS	3899[ii]	1.28[ii]	0.3[ii]	3.2[ii]	2.1[ii]	140[ii]	...	...	183[g]	...	0.6[ii]
116	RY Lup	K4[j]	CTTS	5060[z]	0.65[j]	1.5[j]	2.6[j]	2.6[j]	140[ii]	3.8[j]	38[z]	92[g]	...	0.5[jj]
118	EX Lup	M0.5[ee]	CTTS	3802[ii]	0.00[ii]	0.5[ii]	1.5[ii]	0.4[ii]	140[ii]	...	...	236[g]	...	0.2[ii]
120	HO Lup	M1[ii]	CTTS	3648[ii]	1.25[ii]	0.3[ii]	1.8[ii]	0.5[ii]	140[ii]	...	...	236[g]	...	0.4[ii]
122	HK Lup	K7[ee]	CTTS	3999[ii]	0.82[ii]	0.4[ii]	1.8[ii]	0.6[ii]	140[ii]	...	...	242[g]	...	0.6[ii]
123	Sz 102	K0[ii]	CTTS	5248[ii]	1.13[ii]	...[ii]	0.1[ii]	0.0[ii]	140[ii]	...	...	...	...	1.0[ii]
125	AS 205	K0[t]	CTTS	5248[t]	2.23[c]	2.2[t]	3.5[t]	8.3[t]	160[t]	...	10[l]	116[g]	...	0.8[t]
126	Wa Oph/3	K0[gg]	NTTS	5232[kk]	1.30[gg]	1.6[gg]	2.4[cc]	3.8[gg]	160[gg]	...	77[gg]	106[g]	...	0.0[hh]
127	Sco PMS 060	G0[gg]	NTTS	5948[e]	0.60[gg]	1.6[gg]	1.7[cc]	3.3[gg]	160[gg]	...	35[gg]	0.04[g]	...	0.0[hh]
129	SR 9	K6[j]	CTTS	4650[z]	0.50[j]	1.2[j]	3.5[j]	3.5[j]	170[x]	6.4[j]	24[z]	236[g]	...	0.6[ll]
132	AS 209	K5[l]	CTTS	4395[c]	1.15[c]	1.4	2.4[c]	2.5[c]	160[mm]	...	10[l]	226[g]	...	0.5[oo]
133	AK Sco	F5[mm]	CTTS	6445[e]	...	...	...	...	...	...	...	...	...	...
143	AS 292	K5[mm]	CTTS	4395[b]	...	...	...	...	...	...	...	...	...	...
144	FK Ser A	K5[a]	CTTS	4395[b]	...	...	...	...	...	...	...	...	...	...

TABLE 1—*Continued*

Index	Star	Spectral Type	Class	T_{eff} (K)	A_V (mag)	M_* ($M_\odot$)	R_* ($R_\odot$)	L_* ($L_\odot$)	Distance (pc)	P_{rot} (days)	$v \sin i$ (km s^{-1})	τ_c (days)	$\dot{M}$ ($M_\odot$ yr^{-1})	$\Delta(H-K)$ (mag)
146......	S CrA	K6[ee]	CTTS	4272[mm]	0.50[mm]	0.6[nn]	2.1[mm]	1.3[mm]	130[mm]	...	...	226[g]	...	0.8[oo]
149......	HBC 678	G8[a]		5481[kk]	...	...	...	...	...	...	...	...	...	...
160......	DI Cep	G8[x]	CTTS	5510[mm]	0.90[mm]	1.8[nn]	2.5[mm]	5.1[mm]	300[mm]	...	...	68[g]	...	0.6[oo]

[a] Herbig & Bell 1988.
[b] Assigned from spectral type based on T_{eff}–spectral type relation of note f.
[c] Valenti et al. 1993a, 1993b.
[d] Walter et al. 1988.
[e] Using T_{eff}–spectral type relation from Gray 1992.
[f] Hartigan et al. 1995.
[g] Used tabulated T_{eff} and L_* with pre–main-sequence tracks of D'Antona & Mazzitelli 1994 to estimate ages which are then used with tabulated mass and Gilliland 1986 to estimate τ_c.
[h] Same as note dd but used colors from note i.
[i] Strom et al. 1989.
[j] Bouvier 1990.
[k] Herbst et al. 1987.
[l] Basri & Batalha 1990.
[m] Gullbring et al. 1998.
[n] Used note f to get stellar ages which with the tabulated mass are used to estimate τ_c from Gilliland 1986.
[o] Bouvier et al. 1993.
[p] Used stars in common between notes m and f to compute a correction to values from note f.
[q] Johns-Krull 1996.
[r] Bertout et al. 1988.
[s] Cabrit et al. 1990.
[t] Liu et al. 1996.
[u] Bouvier et al. 1995.
[v] Hartmann et al. 1986.
[w] Giampapa et al. 1981.
[x] Cohen & Kuhi 1979.
[y] Skinner et al. 1991.
[z] Padgett 1996.
[aa] Gauvin & Strom 1992.
[bb] Used tabulated T_* and L_* with HR diagram in note aa to estimate.
[cc] Determined from L_* and T_{eff}.
[dd] Used colors from note aa with tabulated A_V and intrinsic colors from Bessell & Brett 1988 to estimate.
[ee] Appenzeller et al. 1983.
[ff] Lawson et al. 1996.
[gg] Walter et al. 1994.
[hh] Used colors from note gg with tabulated A_V and intrinsic colors from Bessell & Brett 1988 to estimate.
[ii] Hughes et al. 1994.
[jj] Used SIMBAD colors and tabulated A_V with intrinsic colors from Bessell & Brett 1988 to estimate.
[kk] Assigned by averaging like spectral type already in table.
[ll] Used colors from Green & Young 1992 along with tabulated A_V and intrinsic colors from Bessell & Brett 1988 to estimate.
[mm] Hamann & Persson 1992.
[nn] Used tabulated T_{eff} and L_* with pre–main-sequence tracks of D'Antona & Mazzitelli 1994 to estimate mass.
[oo] Used colors from note mm along with tabulated A_V and intrinsic colors from Bessell & Brett 1988 to estimate.

cally range over a factor of 10^2–10^3 for our full sample of TTSs, so the general trends observed should be relatively insensitive to uncertainties in the system parameters.

In Table 1 we also attempt to classify the TTSs as CTTSs or NTTSs. As discussed in § 1, the term CTTS, while originally defined strictly on an observational criteria, has come to be synonymous in the literature with an *accreting* TTS. Therefore, we classify stars as CTTS if they show evidence for ongoing accretion such as optical veiling, redshifted absorption components in their line profiles, or a near-IR excess indicative of a close circumstellar accretion disk. Stars with none of the above three criteria are assumed to be nonaccreting stars and are labeled as NTTSs. Our classification of CS Cha as a CTTS deserves further clarification. Gauvin & Strom (1992) present a spectral energy distribution for CS Cha which shows no near-IR excess out to ~ 10 μm. Gauvin & Strom estimate that an accretion disk with an inner hole, such that there is no dust out to a radius of $\sim 50 R_*$ could explain the lack of near-IR emission. The Hα equivalent width of CS Cha is listed as 13 Å by Gauvin & Strom (1992), which is relatively low but still qualifies the star as a CTTS according to the original observational criteria (Herbig 1962). On the other hand, Reipurth, Pedrosa, & Lago (1996) observe an Hα equivalent width of 54 Å in CS Cha, and the line profile presented by these authors shows hints of a redshifted absorption component in Hα. So, while there may be no dust close to the star, there is plenty of evidence that *gas* accretes onto CS Cha, and hence we classify it as a CTTS.

Below, we will examine the relationship between the dynamo number, N_D, and the UV emission level in TTSs. According to dynamo theory (e.g., Durney & Latour 1978), $N_D \propto 1/R_0^2$, where R_0 is the Rossby number which is simply the rotation timescale divided by the convective timescale and is often defined as $R_0 \equiv P_{rot}/\tau_c$, where P_{rot} is the rotation period and τ_c is the convective turnover time at some representative place in the stellar interior. Therefore, we need estimates of the convective turnover times, τ_c, in TTSs. However, τ_c is a function of depth in the star, so one must specify where to calculate τ_c. It has long been suspected that

TABLE 2

MAIN-SEQUENCE STARS

Star	Number of Spectra	Spectral Type	Distance (pc)	P_{rot} (day)	τ_c (day)	log R'_{HK}	$F_{1958} \times 10^{15}$ (ergs s^{-1} cm^{-2} Å^{-1})	$F_{CIV} \times 10^{13}$ (ergs s^{-1} cm^{-2})	$F_{CII} \times 10^{14}$ (ergs s^{-1} cm^{-2})
BD −09 3468	3	F5 V	22.6	6.9	1.2	−4.65	1170.0(3.0)	0.80(70)	...
AK Her	1	F8 V	95.5	0.4	8.3	...	89.40(40)	1.59(26)	...
EK Dra	15	F8 V	33.9	2.8	13.0	−4.15	29.70(05)	1.82(07)	...
111 Tau	28	F8 V	14.7	3.6	13.0	−4.38	764.00(2.74)	4.51(21)	...
54 Cam	1	F8 V	101.6	10.9	13.0	...	76.30(48)	2.59(33)	...
W UMa	6	F8 V	49.6	0.3	13.0	...	24.20(15)	2.18(23)	...
GJ 334.2	2	F9 V	19.1	9.7	14.5	−4.61	115.00(90)	0.36(25)	...
β Com	4	F9.5 V	9.2	11.2	14.6	−4.76	347.00(1.43)	1.42(15)	...
σ^2 CrB	21	G0 V	21.7	1.1	16.3	...	612.00(69)	18.80(03)	...
ξ UMa B	2	G0 V	...	4.0	16.3	−4.24	1380.0(21.9)	5.36(49)	...
χ^1 Ori	31	G0 V	8.7	5.5	16.3	−4.43	560.00(1.26)	4.67(21)	...
ι Per	4	G0 V	10.5	14.5	16.3	−5.02	455.00(1.39)	0.21(29)	...
ER Vul	22	G0 V	49.9	0.7	16.3	...	82.70(12)	4.73(07)	...
λ Ser	2	G0 V	11.7	25.8	16.3	−5.00	302.0(6.5)	0.48(19)	...
59 Vir A	16	G0 V	18.0	3.3	16.3	−4.45	303.00(52)	4.50(16)	...
HN Peg	11	G0 V	18.4	4.9	16.3	−4.42	160.00(33)	1.34(14)	...
44 ι Boo	32	G0 V	12.8	0.3	16.3	−4.61	243.00(22)	11.70(20)	...
δ Tri	3	G0.5 V	12.2	10.0	17.0	−4.66	352.00(3.22)	1.61(21)	...
π^1 UMa	13	G1.5 V	14.3	5.4	16.8	−4.38	153.00(23)	2.14(13)	...
V502 Oph	1	G2 V	84.5	0.4	18.8	...	10.40(21)	1.81(24)	...
BE Cet	8	G2 V	20.2	7.8	18.8	−4.43	44.60(13)	0.98(15)	...
α Cen A	20	G2 V	1.4	25.0	18.8	−5.00	9000.0(24.2)	19.70(1.80)	...
58 Eri	2	G2.5 V	13.3	7.6	19.2	−4.54	121.00(41)	1.20(37)	...
YY Eri	1	G5 V	55.7	0.3	21.1	...	8.03(18)	0.98(40)	...
κ^1 Cet	14	G5 V	9.2	9.2	21.1	−4.42	160.00(19)	2.54(12)	...
HD 166181	10	G5 V	32.6	1.8	21.1	...	19.40(09)	3.68(11)	...
61 UMa	3	G8 V	9.5	16.7	23.1	−4.55	53.10(30)	1.50(28)	...
V2292 Oph	1	G8 V	16.9	11.4	23.1	−4.45	14.10(15)	0.47(23)	...
SV LMi	1	G8 V	11.2	18.6	23.1	−4.64	20.80(47)	1.09(68)	...
ξ Boo A	53	G8 V	6.7	6.2	23.1	−4.36	116.00(09)	4.82(09)	...
SW Lac	2	K0 V	81.3	0.3	26.1	...	4.24(09)	1.29(11)	0.68(18)
36 Oph A	1	K0 V	6.0	20.7	26.1	−4.56	36.90(21)	2.25(44)	1.91(35)
70 Oph A	12	K0 V	5.1	20.0	26.1	−4.55	67.20(14)	3.87(19)	1.61(24)
VW Cep	41	K0 V	27.7	0.3	26.1	...	5.67(04)	3.34(05)	0.73(08)
HD 86590	9	K0 V	32.4	1.1	26.1	...	4.89(07)	3.87(15)	1.19(13)
XY Leo	1	K0 V	63.1	0.3	26.1	...	0.80(12)	1.00(11)	...
107 Psc	2	K1 V	7.5	35.2	30.2	−4.91	12.70(11)	0.16(12)	0.72(22)
36 Oph B	2	K1 V	6.0	21.1	30.2	−4.56	38.40(18)	2.20(23)	3.22(36)
α Cen B	5	K1 V	1.4	25.0	30.2	−4.92	366.00(1.05)	11.10(1.00)	...
12 Oph	2	K2 V	9.8	21.1	32.6	−4.58	10.50(10)	0.64(11)	1.14(22)
ϵ Eri	62	K2 V	3.3	11.7	32.6	−4.45	57.90(09)	8.39(11)	7.13(18)
EP Eri	7	K2 V	8.3	6.8	32.6	−4.31	8.01(09)	2.09(12)	1.70(19)
GJ 688	1	K3 V	10.7	36.4	35.8	−4.78	1.63(09)	1.95(94)	...
GJ 105 A	1	K3 V	7.8	48.0	35.8	−4.96	2.50(17)	0.22(23)	...
GJ 775	1	K4 V	13.1	29.0	41.0	−4.64	1.61(19)	0.29(09)	1.76(46)
61 Cyg A	11	K5 V	3.5	35.4	46.1	−4.76	2.01(06)	0.53(11)	0.70(15)
EQ Vir	5	K5 Ve	19.8	4.0	46.1	...	1.30(14)	1.38(11)	1.48(32)
61 Cyg B	2	K7 V	3.5	37.8	58.0	−4.89	1.48(16)	0.00(20)	1.32(31)
AU Mic	38	M0 Ve	9.9	4.8	65.0	...	1.45(04)	2.00(07)	0.43(07)
AD Leo	36	M3 Ve	4.8	2.7	73.0	...	1.89(05)	2.60(13)	...
EV Lac	40	M3.5 Ve	5.0	4.4	76.0	...	0.93(04)	2.03(10)	0.54(08)

the solar dynamo is located right at the base of the convection zone where strong radial sheer can exist between this region and the radiative core. On the other hand, the majority of the TTSs are expected to be fully convective (D'Antona & Mazzitelli 1994), leaving us in a quandary as to where to evaluate τ_c. In fact, because most TTSs are fully convective, the nature of the dynamo acting in these stars is probably more like a turbulent dynamo (Durney, De Young, & Roxburgh 1993) instead of the traditional solar like $\alpha - \Omega$ dynamo, making the traditional dynamo number no longer necessarily the correct quantity to consider. Nevertheless, we explore relationships with Rossby number to see what results.

The most recent work on computing convective turnover times in pre–main-sequence stars is that of Kim & Demarque (1996); however, they consider a relatively small range in mass which would severely limit the size of the sample we can use from our *IUE* observations. Therefore, we use the work of Gilliland (1986) to estimate τ_c for both the TTSs in our *IUE* sample (given in Table 1) as well as for

TABLE 3

EVOLVED STARS

Star	Spectral Type	Distance (pc)	P_{rot} (days)	τ_c (days)	R_* ($R_\odot$)	$F_{CIV} \times 10^{13}$ (ergs s^{-1} cm^{-2})
HD 155555	G5 IV + K0 IV–V	45.0	1.7	60.3	2.3	7.1
AR Lac	G2 IV + K0 IV	49.0	2.0	91.4	3.1	12.0
HR 1099	G5 IV + K0 IV	36.0	2.8	164.9	2.8	31.0
θ Dra	F8 IV–V	14.5	3.1	18.7	1.8	8.2
TY Pyx	G5 IV + G5 IV	57.0	3.2	103.5	1.6	7.0
SZ Psc	F8 V + K1 IV	89.0	3.9	76.0	4.0	4.3
Z Her	F4 V–IV + K0 IV	82.0	4.0	91.6	2.6	1.9
UX Ari	G5 V + K0 IV	57.0	6.4	90.4	3.9	14.0
II Peg	K2.5 IV–V	72.0	6.7	71.8	3.7	9.6
α Aur	F9 III + G6 III	13.2	9.0	167.6	7.3	440.0
1 Gem	F5 V + G5 II	56.0	9.6	264.4	12.0	1.0
42 Cap	G2 IV	30.0	13.2	123.2	3.0	5.4
6 Tri	G5 III + G5 III	115.0	14.7	131.0	12.0	2.7
ζ And	K1 II + K0 V	50.0	17.8	40.8	12.5	6.7
σ Gem	K1 III	59.0	19.6	72.8	15.0	31.0
HK Lac	FIV + K0 III	130.0	24.4	80.8	15.0	3.0
HR 8703	K1 IV–III	59.0	24.6	20.5	10.0	18.7
HR 7275	K1 IV	57.0	28.6	90.4	8.0	9.2
λ And	G8 IV–III	30.0	53.7	295.1	7.9	26.0
HR 4665	K0 III + K0 III	130.0	64.4	117.2	15.0	6.4
12 Cam	K0 III	134.0	80.2	298.0	16.0	6.0
HR 7428	A8 IV + K	165.0	108.6	184.4	26.0	2.6
o Dra	K0 III–II	54.0	137.4	92.9	14.0	2.3

the main-sequence stars we compare with. We note that for models in common between Gilliland (1986) and Kim & DeMarque (1996), the Kim & DeMarque (1996) convective turnover times are about 30% greater than those of Gilliland (1986) for TTSs. Given that the TTSs are already in the saturated regime of Dynamo numbers (see below), the Kim & DeMarque (1996) turnover times would just make them more saturated and have no effect on our basic results. Computation of τ_c using Gilliland (1986) requires an estimate of the mass and the age of the star in question. We take the masses from Table 1 and the ages (based on evolutionary tracks of D'Antona & Mazzitelli 1994) from Hartigan, Edwards, & Ghandour (1995) where appropriate. For those stars not listed in Hartigan et al., we take the mass and luminosity estimates in Table 1 and use the D'Antona & Mazzitelli (1994) isochrones to estimate the age ourselves. As described below, the convective turnover times used for the RS CVn stars come from Basri (1987) using the work of Gilliland (1985). The two Gilliland (1985, 1986) papers use the same convective model applied to stars at different evolutionary states, providing a uniform theoretical estimate of τ_c for all the stars in our sample.

2.3. *Dwarf and RS CVn Comparison Stars*

As is well known, late-type dwarf and subgiant stars also show substantial emission in many of the lines found in the bandpass covered by the *IUE* short-wavelength primary (SWP) camera. These emissions appear related to their dynamo-generated magnetic activity (e.g., Vilhu 1984). In order to compare the behavior of the SWP emissions seen in TTSs with those of magnetically active main-sequence and RS CVn "standard" stars, we have compiled a list of main-sequence comparison stars taken from the sample of Vilhu (1984) and supplemented with several additional stars from the Mount Wilson Ca H and K long-term monitoring program (e.g., Duncan et al. 1991; Baliunas et al. 1995; Henry et al. 1996). These stars are presented in Table 2. Additionally, we have compiled data on a handful of active M dwarfs since many of the TTSs in our sample are of spectral type K7 or later. The data for these stars are also listed in Table 2.

Table 2 lists the distance to each star, as well as the convective turnover time, τ_c, for each star. The distances used here are taken from the *Hipparcos* on-line database, and the values of τ_c are taken from Gilliland (1986) as described above for the TTSs. Finally, Table 2 also lists the continuum surface flux at 1958 Å and the integrated C IV 1549 Å and C III 1909 Å surface fluxes for each star. These quantities were measured in the same way as was done for the TTSs in our sample (Paper I). Short-wavelength spectra from the *IUE* final archive were again used, and in the case where multiple spectra exist for a given target, we use the same weighted mean averaging technique described by Valenti at al. (2000) to combine the spectra. In general, we considered all available *IUE* SWP spectra for each object, except in a few cases such as HR 1099 where a tremendous number of observations are available. In most cases the C III 1909 Å line was too weak to reliably measure. The second column of Table 2 gives the total number of spectra considered for each star in the sample. To construct the surface flux from the measured *IUE* fluxes and *Hipparcos* distances, stellar radii for the main-sequence stars are taken from the tables in Gray (1992) based on spectral type.

The TTSs we wish to study have substantially deeper convection zones than main-sequence comparison stars of similar spectral type. The RS CVn stars are late-type evolved stars which also have deeper convection zones than their main-sequence counterparts. Therefore, the RS CVn stars may provide a better benchmark of the dynamo related activity expected on TTSs. We have also compiled a list of RS CVn "standard" stars given in Table 3. Stellar parameters and *IUE* C IV line flux measurements are taken from Basri, Laurent, & Walter (1985) and Basri (1987). The convective turnover times given in Basri (1987) are based on the theoretical calculations of Gilliland (1985) which uses the same modeling formulation as Gilliland (1986). Since we use Gilliland (1986) to estimate the convective turnover times of the main-sequence dwarfs and the TTSs, we have self-consistent theoretical estimates of this quantity for all the stars considered in this paper.

3. ANALYSIS

In most other classes of late-type active stars, emission seen in the SWP band of *IUE* is attributed to nonradiative heating by surface magnetic fields (we discuss "basal" heating below as well). While TTSs do appear to have strong surface magnetic fields (Johns-Krull & Valenti 2000), CTTSs are also accreting material from their surrounding accretion disk which provides another source of available energy. By comparing the properties of the emission observed from TTSs internally and with other properties of these stars, we hope to see to what extent magnetic and accretion related phenomena are responsible for the observed emissions.

3.1. *SWP Line & Continuum Correlations*

We first looked to see if the line and continuum emission recorded in the *IUE* SWP spectra are correlated with one another. In doing this comparison, one can compare either surface fluxes or luminosities, and it is not necessarily required that a correlation in one quantity implies a correlation in the other. As it turns out for the TTSs in our sample, all the measured line and continuum emissions are well correlated in both luminosity and surface flux. Several examples are shown in Figure 1. The first panel of plots shows the 1958 Å continuum luminosity on the abscissa compared with the other continuum and line luminosities. In each case the solid circles show the CTTSs, and the asterisks show the NTTSs in our sample. Recall that for each star, the flux determined from the weighted mean spectrum is used (see Paper I). Only 3 σ or better detections are plotted in these figures.

For the CTTSs, all lines and continua appear to be well correlated with one another, with the possible exception of the H_2 $\lambda1503$ line. For every possible pair of line and continuum luminosities, we calculate the linear correlation coefficient and its associated false alarm probability (Bevington & Robinson 1992). In these calculations we use the log of the luminosity (or surface flux). The correlation coefficient alone cannot be used directly to test for the existence of a correlation, since in the limit of small sample sizes, it is likely that two random populations will produce a relatively large linear correlation coefficient. The false alarm probability (FAP) is a measure of how likely it is that two random vectors of the given length will produce a linear correlation coefficient equal to or greater than the measured value. Small numbers indicate a significant correlation. As such, the FAP is the quantity that should be compared when deciding if two data sets show a correlation. In our *IUE* sample, the lowest FAP ($f_p = 1.9 \times 10^{-20}$) is obtained when comparing the 1760 Å continuum surface flux versus the 1958 Å continuum surface flux (when the comparing luminosities the $f_p = 7.9 \times 10^{-20}$). For most line or continuum pairs, the CTTSs give $f_p \sim 10^{-7}$–10^{-11}, all indicating a high degree of correlation. The exception to this is the H_2 $\lambda1503$ molecular hydrogen line.

As shown in Figures 1*f* and 1*m*–1*v*, the H_2 $\lambda1503$ line does appear well correlated with the other line and continuum emission, but the FAP associated with these correlations is substantially higher due to the relatively small number of CTTSs in which molecular hydrogen emission was detected (Paper I). The best correlation with the H_2 $\lambda1503$ line is the emission in the $\lambda1296$ line of S I, yielding a FAP of 2.2×10^{-4} (see Fig. 1*m*). The FAP is defined so that a value of $f_p \leq 10^{-2}$ will result $\sim1\%$ of the time from uncorrelated data that are distributed in a normal fashion. The occurrence rate roughly doubles for uniform distributions. The weakest correlation is with the pair of Si IV lines at 1394 and 1403 Å, resulting in a FAP of 1.1×10^{-2}, which still indicates a high degree of correlation. The picture is nearly the same if the $\lambda1530$ line of H_2 is used instead, but this time the weakest correlation is with the He II line at 1640 Å. Only four CTTSs showed emission in additional molecular hydrogen lines, and it is no longer profitable to explore correlations with such small statistics.

These correlations suggest that all of the emissions shown share a common origin in the stellar systems. For the atomic lines, this is not too surprising since most of the lines seen in the *IUE* SWP form in "transition region" material with a characteristic temperature of $\sim10^5$ K, and so the various lines are expected to scale with one another. However, it is unlikely that the continuum is forming in $\sim10^5$ K gas (see more below), so it is not necessarily expected that the lines and continuum luminosities (or surface fluxes) should be well correlated. In fact, in the case of main-sequence stars, there is a much weaker correlation between the surface flux in the C IV line and the 1958 Å continuum for the stars shown in Table 2. For the main-sequence stars, the correlation coefficient between the two surface fluxes is 0.55 with a FAP of 2.3×10^{-5}. Haisch & Basri (1985) also find a correlation between the ~2000 Å continuum and C IV line emission in a sample of main-sequence stars, but with considerable scatter in the data. For the CTTSs in our sample, the short-wavelength continuum and C IV line surface fluxes produce a correlation coefficient of 0.93 with a FAP of 7.1×10^{-13}. In the case of main-sequence stars, it is believed that the heating associated with the magnetic fields produces a slight temperature increase in the temperature minimum region, raising the continuum brightness near 2000 Å. Heating associated with the same magnetic fields also produces the 10^5 K gas in the transition region, resulting in emission from lines such as C IV and producing the correlation (e.g., Simon et al. 1985; Haisch & Basri 1985). The same scenario could be at work in the TTSs; however, the much tighter correlation seen in these stars hints that a more direct relationship may be present.

Surprisingly, the molecular hydrogen lines are also well correlated with all the other emission traced by *IUE*. The H_2 emission cannot arise in the same gas producing the continuum or other line emission since molecular hydrogen does not survive to these high temperatures. It is believed that the H_2 emission is the result of fluorescence from a thermally excited state (probably produced in wind and/or accretion shocks in the molecular material surrounding the CTTSs). The primary pump is Lyα (Paper I). Unfortunately, the Lyα in our TTS *IUE* spectra is contaminated with geocoronal emission and cannot be reliably measured;

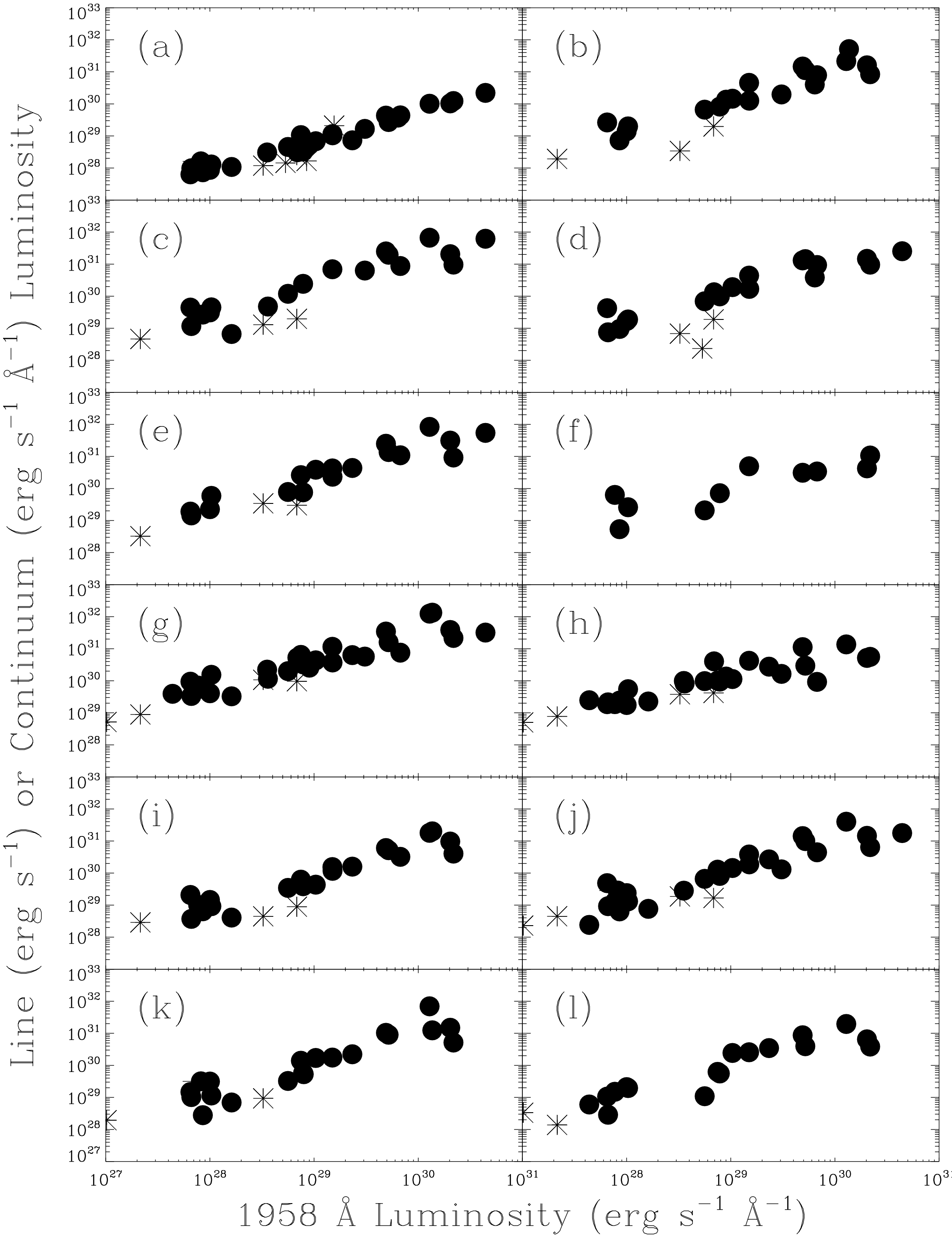

FIG. 1.—Correlations of the extinction corrected line and continuum luminosities in our sample of TTSs. In panels (*a*)–(*l*), the abscissa is the 1958 Å continuum luminosity. The ordinate in each panel is as follows: (*a*) 1760 Å continuum, (*b*) S I 1296 Å line, (*c*) O I 1304 Å line, (*d*) Si II 1309 Å line, (*e*) Si IV 1394 plus 1403 Å lines, (*f*) H_2 1503 Å line, (*g*) C IV 1549 Å line, (*h*) He II 1640 Å line, (*i*) Si II 1808 Å line, (*j*) Si II 1817 Å line, (*k*) Si III 1892 Å line, and (*l*) C III 1909 Å line. The CTTSs are plotted as solid circles and NTTSs are plotted as asterisks. In panels (*m*)–(*v*) several lines are also plotted vs. the molecular hydrogen emission at 1503 Å on the abscissa. The ordinates in these panels are as follows: (*m*) S I 1296 Å line, (*n*) O I 1304 Å line, (*o*) Si II 1309 Å line, (*p*) Si IV 1394 plus 1403 Å lines, (*q*) C IV 1549 Å line, (*r*) He II 1640 Å line, (*s*) Si II 1808 Å line, (*t*) Si II 1817 Å line, (*u*) Si III 1892Å line, and (*v*) C III 1909Å line. Only CTTSs appear in these panels since they are the only objects with detectable H_2 emission. In all the panels, only stars with 3 σ detections in all relevant emissions are show; therefore, there are differing numbers of points in the various panels. Error bars are included on both axes, but the error bars are generally smaller than the plot symbols.

however, it is expected that Lyα emission is correlated with the other high-temperature emissions shown in Figure 1. Therefore, the correlation between H_2 and these other lines is probably due to the general correlation between Lyα and these other high-temperature emissions.

3.2. *The Short-Wavelength Continuum*

Tabulated in Paper I is the mean continuum flux at 1760 Å and the mean continuum flux at 1958 Å. The correlation between these two continua is quite good as can be seen in

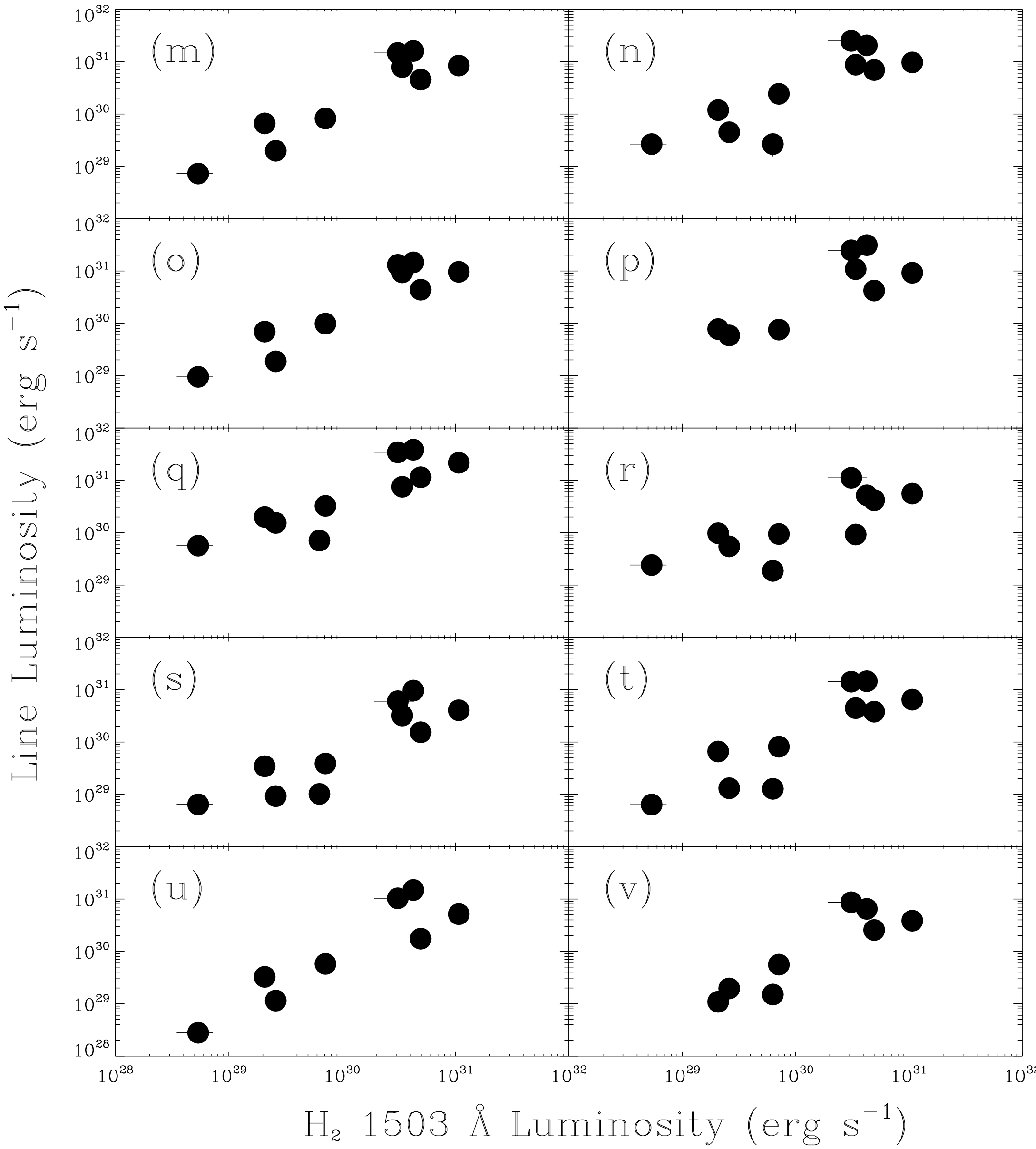

FIG. 1.—*Continued*

Figure 1*a*. In Figure 2 we reproduce this figure (this time showing surface fluxes instead of luminosities) along with the positions of blackbodies at a range of temperatures between 4500 and 11,000 K. As in all plots, the stellar emission quantities are corrected for extinction. Also shown are two lines representing the ratio of the two fluxes for blackbody emitters at 10,000 K (*upper dashed line*) and 4500 K (*lower dashed line*). For comparison, it is noted that the brightness temperature of the quiet Sun below 2000 Å is 4500 K (Feldman & Doschek 1978; Vernazza, Avrett, & Loeser 1981; Cook, Brueckner, & Bartoe 1983), and the brightness temperature of solar plage regions below 2000 Å is $\sim$4800 K (Feldman & Doschek 1978; Cook, Brueckner, & Bartoe 1983). For a sample of active and inactive G0–G5 main-sequence stars, Haisch & Basri (1985) find brightness temperatures of 4450–5100 K.

It should be kept in mind that the positions of the blackbodies (*squares*) in Figure 2 are for a filling factor of 1.0. Thus, a TTS surface flux coincident with any particular square indicates that emitting material at the specified temperature covers the entire surface of the TTSs. For lower filling factors, the brightness temperature in any given band decreases, but the color temperature implied by the ratio of fluxes in the two bands remains constant, assuming negligible UV contribution from the remainder of the stellar surface.

Unfortunately, there are only a few NTTSs in this plot. This is because a relatively small number of NTTSs were observed by *IUE* in this wavelength range, and several that were observed were not detected, particularly in the continuum. The few NTTSs that were detected tend to be the brighter, relatively early spectral type members of this group. In fact, the average effective temperature of the NTTSs shown in Figure 2 is 5534 K. The blackbody temperature derived from the mean of the NTTS flux ratios is nearly identical to the actual mean effective temperature of these stars.

As mentioned above (and described more fully below), NTTSs are expected to be very magnetically active, so the brightness temperatures of these stars at 2000 Å are

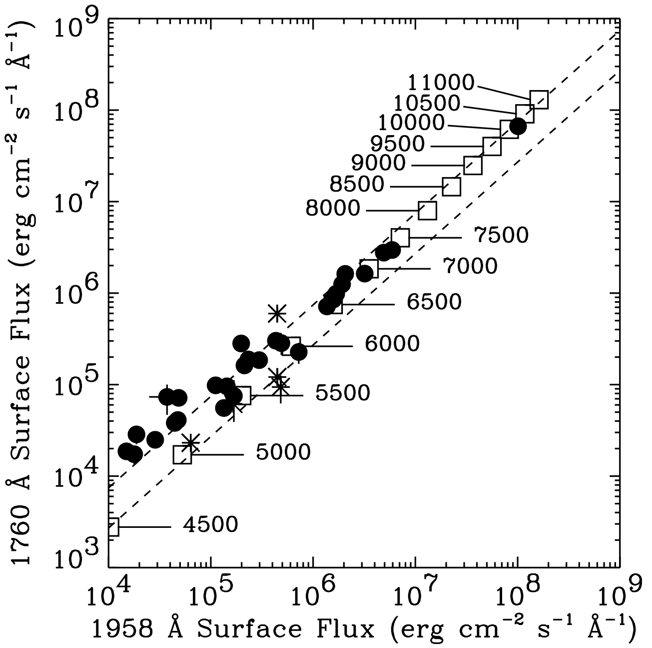

FIG. 2.—Mean continuum surface flux around 1760 Å plotted vs. the mean continuum surface flux near 1958 Å for the TTSs in our sample. The CTTSs are shown in solid circles, and the NTTSs are shown in asterisks. Error bars for both samples are included. The positions of blackbody emitters are also shown in the plot with squares labeled by the appropriate temperature in degrees Kelvin. Additionally, the upper dashed curve shows the locus of flux ratios for a 10,000 K source, and the lower dashed line shows the flux ratios for a 4500 K source.

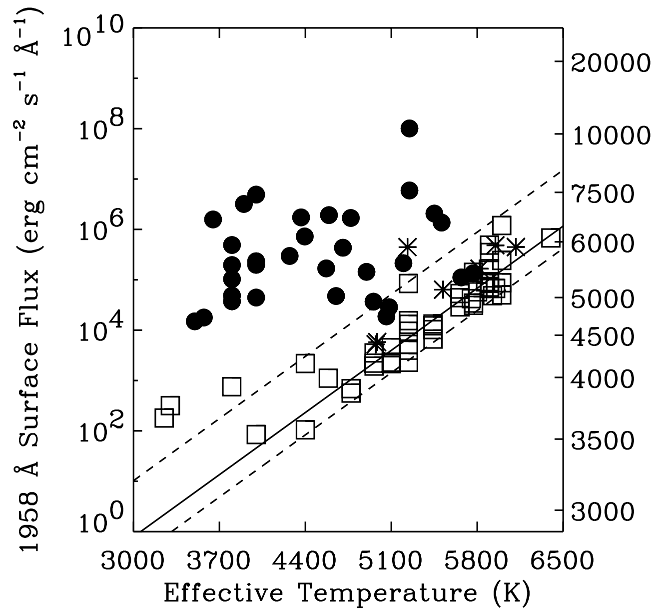

FIG. 3.—Mean continuum surface flux around 1958 Å plotted vs. the stellar effective temperature. Again, the CTTSs are shown in solid circles, and the NTTSs are shown in asterisks, with error bars included on the plot. The main-sequence stars from Table 2 are shown with squares. The solid line shows a least squares fit to the main-sequence stars, and the two dashed curves encompass the lower and upper bounds of the main-sequence stars.

unknown. Nevertheless, the solar analogy and the stellar data shown in Figure 3 (described below) and given in Haisch & Basri (1985) suggest that the brightness temperature below 2000 Å should be approximately equal to, or a little below, the stellar effective temperature. With the exception of one star (Wa Oph/3) the NTTS flux ratios seem to bear this out, implying the short-wavelength continuum observed by *IUE* for these stars is produced by the magnetically active stellar photosphere. Wa Oph/3 is a generally unremarkable NTTSs, showing typical levels of X-ray, Hα, and Ca II H and K emission (Walter 1986; Walter et al. 1994). It was found by Ghez, Neugebauer, & Matthews (1993) to be a close binary (0".208 separation—30 AU—with a flux ratio of 4 in the K band). Since it was only observed once, it is possible a flare is responsible for its enhanced emission. It should be observed again to verify its quiescent emission level.

On the other hand, the CTTS mean flux ratio implies a color temperature of $\sim$10,000 K, a value much higher than the mean effective temperature for these stars ($\sim$4000 K). This is, however, similar to the temperature deduced spectroscopically for the accretion shocks responsible for the optical veiling emission (Basri & Bertout 1989; Hartigan et al. 1991; Valenti et al. 1993a). It would therefore appear that the 1700–2000 Å continuum in CTTSs is formed in the same postshock gas producing the optical veiling. This reinforces the conclusions drawn by Herbig & Goodrich (1986) in their optical-UV study of five TTSs.

Another way to visualize the behavior of the short-wavelength continuum of TTSs is shown in Figure 3. Here the 1958 Å continuum surface flux is shown as a function of stellar effective temperature. Along with the TTSs are plotted the main-sequence stars from Table 2. These standard stars span a large range in activity level; however, they generally fall below the TTSs in 1958 Å continuum surface flux, particularly at the lower effective temperatures. The short-wavelength continuum surface flux of these standard stars correlates very well with effective temperature above about 4900 K and seems to show little correlation with effective temperature below this value, though there are relatively few of these cooler stars. The solid line in Figure 3 is a linear fit to the standard stars above 4900 K, and the two dashed lines are this same fit offset so that they encompass all the standard stars above 4900 K. At any given effective temperature, the range of continuum surface flux values is presumably due to differences in magnetic activity (e.g., Simon et al. 1985), which in turn is due to differences in rotation which drives the dynamo (e.g., Vilhu 1984; Noyes et al. 1984). These lines encompass all but three of the standard stars at effective temperatures below the range used in the fit, with the three exceptions among the most active dMe flare stars: EV Lac, AD Leo, and AU Mic.

While several of the TTSs fall close to or within these lines, the vast majority of them do not. The cooler TTSs (all CTTSs) fall well above the range expected from the standard stars by at least 1.5 orders of magnitude. As we will see below, the main-sequence stars in Figure 3 span a range in dynamo number with values well above (and below) those of the TTSs. Therefore, it is unlikely that magnetic processes can be responsible for the excess continuum of the all the TTSs, especially the cooler CTTSs. Therefore, we must look for a different explanation for the strong short-wavelength continuum emitted from TTSs, and we will return to this point below in our discussion of accretion-related emission.

3.3. *Dynamo Origin of the IUE Emissions Seen in TTSs?*

While accretion-related processes probably contribute to the CTTS emission lines observed by *IUE* (e.g., Calvet et al.

1996), it is generally believed that the short-wavelength emission from main-sequence stars observed by *IUE* is related to surface magnetic activity. Given the strong magnetic fields observed on some TTSs (e.g., Johns-Krull, Valenti, & Koresko 1999; Johns-Krull & Valenti 2000), similar emission may also exist on these stars. This magnetic activity is thought to be related to the rotation of the star through a magnetic dynamo process. The strong effective temperature dependence of the continuum surface flux (Fig. 3) makes studying this phenomena in the continuum difficult; however, much success has been achieved by studying the emission lines observed in the *IUE* short-wavelength bandpass (e.g., Vilhu 1984). Therefore, we will focus our discussion on the emission lines, particularly C IV which is bright in the TTSs and well studied among the main-sequence reference stars.

In addition to a magnetic source of heating for chromospheric and transition region lines, there has been a great deal of work on the "basal" level of heating in the outer atmospheres of stars, perhaps due to the steepening and eventual shocking of acoustic waves generated in the outer convection zones of these stars. Originally, Schrijver (1987) found that the level of "basal" emission in the C IV line was insignificant; however, more recent work by Rutten et al. (1991) indicates a significant level of "basal" emission in the C IV line. Very recently, Judge & Carpenter (1998) have challenged the acoustic origin of this "basal" heating, suggesting the heating really is magnetic in origin. Nevertheless, we examine rotation-activity relationships, with and without corrections for "basal" heating.

3.3.1. *Relationship to Rotation Period*

As has been mentioned before, the high-temperature emission observed in the *IUE* short-wavelength bandpass is well correlated with the stellar rotation rate for main-sequence stars (Vilhu 1984; Simon et al. 1985). Faster rotating stars have higher surface fluxes in the transition region lines. Rapid rotation is believed to enhance the dynamo generation of magnetic fields, and these fields heat gas to transition region temperatures. There remains some dispute as to the functional dependence of observed diagnostics on rotation.

Mean field (or $\alpha - \Omega$) dynamo theory (e.g., Durney & Latour 1978) finds that the generation of magnetic activity is proportional to the dynamo number N_D, which is in turn proportional to the inverse of the Rossby number squared ($N_D \propto R_0^{-2}$). Therefore, the Rossby number is a natural choice as a variable against which to compare various magnetic related phenomena, such as emission in magnetically heated lines. On the other hand, Basri (1987) and Stepién (1994) have looked at the data itself to see if there is a compelling argument to favor the Rossby number over the rotation period alone as the proper stellar parameter to be used in magnetic activity studies. Basri (1987) notes that the Rossby number does better at unifying the behavior of single dwarfs and evolved, late-type binaries, but that rotation period alone is just as good when examining only single dwarfs. Stepién (1994) finds that the Rossby number does improve the situation for a narrow range of dwarfs ($0.5 \leq B-V \leq 0.8$), but that outside this range and when considering giants, the Rossby number is not favored over the rotation period. Therefore, we are lead to consider correlations of the TTS emission with both Rossby number and rotation period alone.

Figure 4 shows the relationship between rotation period and C IV surface flux for our sample of TTSs, as well as for a sample of low-mass main-sequence stars (Table 2) and RS CVn stars (Table 3). The horizontal, dashed line in the figure shows the maximum level achieved by the non-TTS "standard" stars. This level is typically identified as the saturation level of magnetic activity. In this plot, a basal level of C IV flux has been subtracted off the standard stars following the results of Rutten et al. (1991); however, this basal level has only a very small effect (generally less than a symbol size) on only the stars with the lowest C IV flux. Inclusion of basal flux in no way affects the basic appearance of Figure 4 or Figure 5 below.

The dwarfs, as already discussed, show a good correlation between rotation rate and transition region line flux up to the saturation level. The RS CVn stars also show a good correlation with rotation period; however, the relationship between rotation and C IV surface flux appears to be offset from that defined by the dwarf stars. Though we only have three NTTSs in our sample with all the required measurements to be placed on this plot, they appear to obey the same general relation defined by the dwarf stars and lend further support to the idea that the NTTSs are simply very magnetically active stars as a result of very rapid rotation. On the other hand, the CTTSs in Figure 4 do not appear to show any correlation with rotation rate, though the range in observed rotation periods is not large. Their C IV surface fluxes are systematically higher, by about a factor of 40, relative to the main-sequence star surface fluxes, and are about a factor of 10 stronger on average than the RS CVn stars with similar rotation periods. As discussed above,

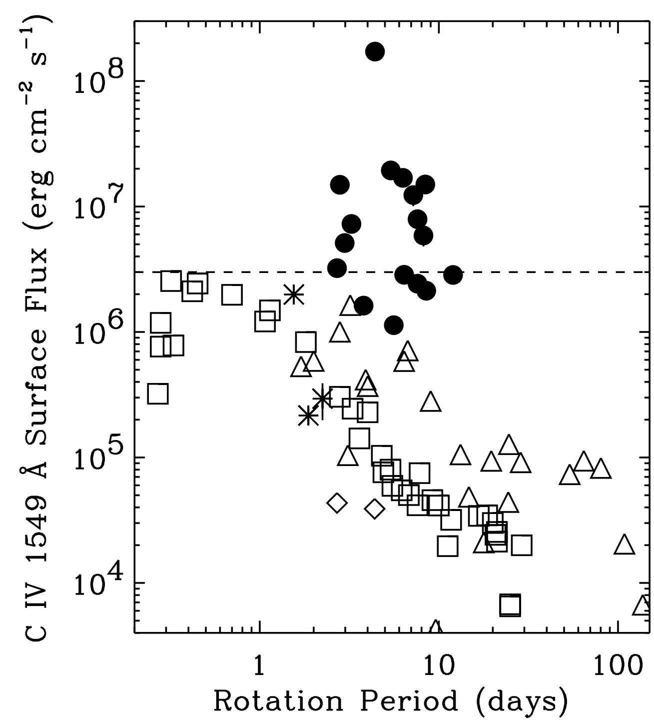

FIG. 4.—C IV 1549 Å surface flux vs. rotation period for our sample of CTTSs (*solid circles*) and NTTSs (*asterisks*). Also shown is a sample of solar type main-sequence dwarfs (*squares*) from Table 2 and a sample of RS CVn stars (*triangles*) from Table 3. The two fully convective M dwarfs from Table 2 are shown as diamonds. The dashed line shows the upper envelope of emission produced by the dwarfs and RS CVn star, which we identify as the activity saturation level.

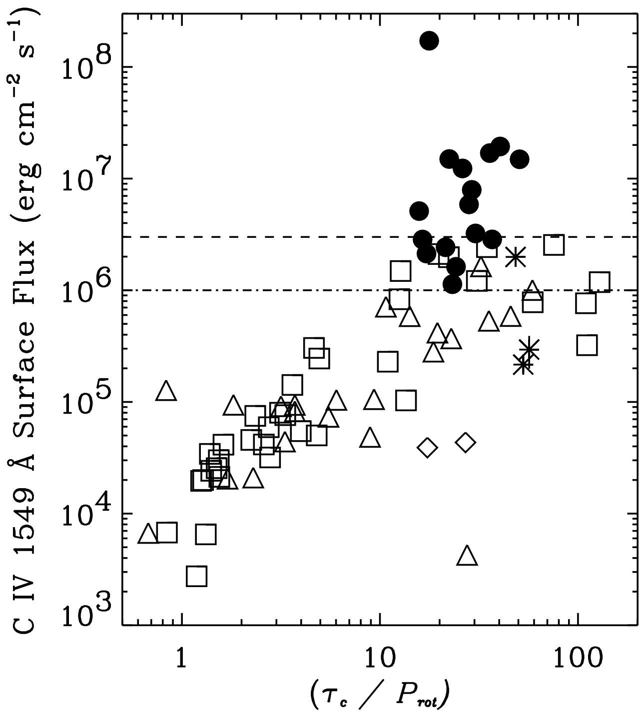

FIG. 5.—C IV surface flux vs. $\tau_c/P_{\rm rot}$ (proportional to the dynamo number). The plot symbols are the same as those of Fig. 4. The dashed line is the saturation level adopted for dwarf stars, and the dashed-dotted line is the activity saturation level adopted for TTSs and described in the text.

the nature of the dynamo may be very different in fully convective TTSs compared to dwarfs. The deeper convection zones of RS CVn stars make them more appropriate analogs of magnetic activity for the TTSs; however, the RS CVn star C IV surface flux also correlates with rotation period, and there is no hint of such a correlation in the TTSs in Figure 4. We searched for correlations between other *IUE* SWP emission quantities and the rotation rate of TTSs and found none.

3.3.2. *Relationship to Dynamo* (*Rossby*) *Number*

As mentioned above, theory suggests that indicators of magnetic activity should better correlate with the Rossby number instead of the rotation period alone. Empirically, Noyes et al. (1984) showed that the Ca II H and K emission in main-sequence stars is better correlated with the inverse Rossby number than with rotation period alone. Vilhu (1984) has shown that the high-temperature emissions traced by *IUE* in late-type stars are also well correlated with inverse Rossby number; and that below a critical Rossby number, the emission level saturates, showing no increase with further decrease in the Rossby number. Figure 4 shows that both the main-sequence star and the RS CVn star C IV surface fluxes correlate well with their rotation rates, but the two groups follow different relationships. Vilhu (1984) showed that these two groups follow essentially the same relationship when the Rossby number is used instead. In the case of the TTSs in Figure 4, their convective turnover times are much longer than for the main-sequence stars, making their Rossby numbers smaller than the main-sequence stars. A smaller Rossby number implies a higher dynamo number and hence more activity, thus we must consider the possibility that the hyperactivity of the CTTSs is due to dynamo-driven magnetic fields.

Figure 5 shows the relationship between the C IV surface flux and $\tau_c/P_{\rm rot} \equiv 1/R_0$ for all the stars shown in Figure 4. The plot symbols are the same as those in Figure 4. At values of $\tau_c/P_{\rm rot} \lesssim 10$, both the main-sequence star and the RS CVn star C IV surface fluxes are well correlated with $\tau_c/P_{\rm rot}$, and both groups appear to follow essentially the same relationship. A little above $\tau_c/P_{\rm rot} \sim 10$, the C IV surface fluxes in these standard stars flatten out as they reach the saturation level. While there are only two fully convective M dwarfs in this sample, they both fall well below this saturation level despite their high values $\tau_c/P_{\rm rot}$. Due to their large convective turnover times, all the TTSs lie in the saturated regime of $\tau_c/P_{\rm rot}$-values despite their relatively long rotation periods. The three NTTSs in the sample lie right in among the saturated standard stars in terms of their C IV surface flux, with two of them possibly being a little low. The CTTSs all lie at or well above this saturated level. It should be noted that for the CTTSs we are generally using the extinction estimates of Gullbring et al. (1998), which are lower on average than previous estimates by Hartigan et al. (1995). Using the Hartigan et al. extinction estimates would increase the difference in C IV surface flux between the CTTSs and the standard stars.

It is apparent from Figures 4 and 5 that the CTTSs do not obey the general relationship between C IV surface flux and rotation and convective parameters. This suggests that in many CTTSs, a significant fraction of the C IV emission is generated by a mechanism other than dynamo-induced magnetic activity. As has been mentioned before, the fully convective nature of TTSs might mean that the dynamo acting in these stars may be very different from that acting in the main-sequence and RS CVn "standard" stars considered here. On the other hand, it has long been held that the activity of NTTSs is simply due to dynamo-generated magnetic fields. Therefore, the NTTSs are the best analogs to the CTTSs when trying to disentangle the affects of traditional stellar activity from other processes such as accretion. Unfortunately, we are only able to place three NTTSs in Figures 4 and 5. We can add one additional NTTS if we look only at C IV surface flux as a function of effective temperature in TTSs (thus abandoning the need for a measure of the rotation period). Figure 6 shows this comparison between CTTSs and NTTSs. Again, the CTTSs are shown as filled circles; 3 σ upper limits for two CTTSs are shown as open circles; and the NTTSs are shown as asterisks (all observed NTTSs were detected in C IV). As a group, the CTTSs are definitely stronger in their C IV emission than the NTTSs, again indicating an emission mechanism other than magnetic activity, operating in many CTTSs. While all these plots and the discussion have focused on C IV emission, the same results are reached when looking at any of the "transition" region lines observed in the *IUE* SWP.

3.4. *Relationship to Accretion*

The primary characteristic that sets the CTTSs apart from NTTSs and main-sequence dwarfs is that the CTTSs are currently undergoing accretion. While there are many estimates of the accretion rate onto CTTSs from the IR (e.g., Cabrit et al. 1990) to the optical (Valenti et al. 1993a; Hartigan et al. 1995; Gullbring et al. 1998), it is generally believed that accretion rates derived from the optical are more accurate as these trace the material actually accreting onto the star. The two large surveys by Valenti et al. (1993a) and

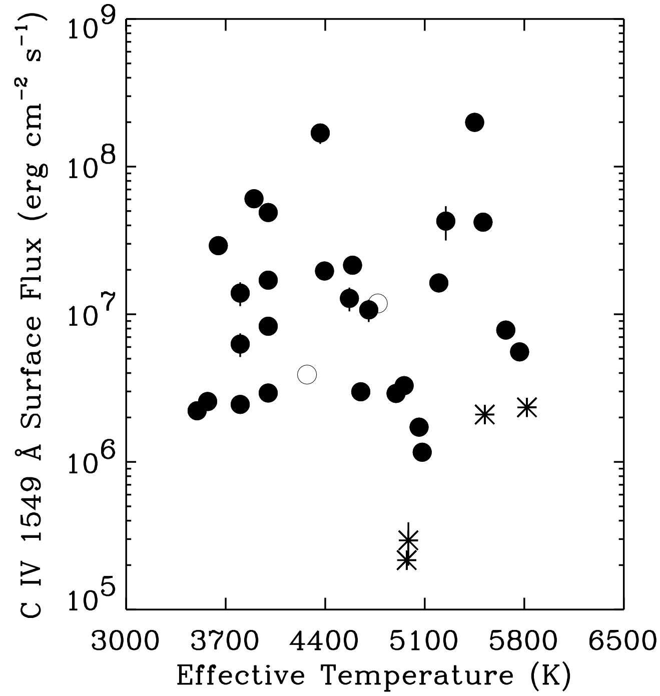

FIG. 6.—Comparison of C IV surface flux in NTTSs and CTTSs as a function of stellar effective temperature. CTTSs are shown as solid circles, NTTSs are shown as asterisks, and 3 σ upper limits for two additional CTTSs are shown as open circles.

Hartigan et al. (1995) derive mass accretion rates from optical observations, though in the first case low-resolution spectroscopy is used to fit the behavior of the continuum from 3400–5000 Å, while in the second case the optical veiling was measured from high-resolution spectra over a narrow wavelength range centered on 5700 Å. The observations for these two studies are from completely different epochs, and it is well known the CTTSs are quite variable. Nevertheless, there is a good correlation between the accretion rates derived in these two studies. However, the accretion rates derived by Hartigan et al. (1995) are systematically higher by about a factor of 10 than the Valenti et al. estimates. While a reexamination of the problem by Gullbring et al. (1998) yielded mass accretion rates closer to those of Valenti et al., we use the Hartigan et al. rates (which are in Table 1) because there is more overlap in the Hartigan et al. sample with our *IUE* sample.

Accretion onto CTTSs is known to produce optical and near-UV continuum radiation characteristic of 10,000 K gas; however, studies of X-rays from CTTSs fail to find convincing evidence that accretion onto CTTSs produces significant amounts of 10^6 K gas. Emission from C IV and the other "transition region" lines found in *IUE* SWP spectra are characteristic of gas at a temperature of 10^5 K, and it is fair to ask whether accretion onto CTTSs is expected to produce such high-temperature material. Using equations appropriate for a strong shock, Calvet & Gullbring (1998) show that accreting material on a typical CTTS ($M_* = 0.5\ M_\odot$, $R_* = 2\ R_\odot$; appropriate for BP Tau for example) is shock heated to 8.6×10^5 K. This value assumes the material essentially falls freely from a distance of $5R_*$, which is identified as the inner truncation radius of the accretion disk in the magnetospheric accretion model. On the other hand, Ostriker & Shu (1995) have actually solved the equations of motion for the gas flow in the magnetospheric accretion flow and find maximum accretion velocities just before the material reaches the stellar surface which are substantially below this value. We will return to this point later; however, it does appear that there is plenty of energy available to heat accreting material to the $\sim 10^5$ K required to produce most of the lines observed in the *IUE* SWP.

As shown in Figure 5, some CTTSs may derive a significant fraction of their C IV luminosity from magnetic heating. Earlier, we identified the upper envelope of magnetically produced C IV emission (the saturation level) with the upper envelope displayed by the main-sequence and RS CVn "standard" stars (the horizontal dashed line in Fig. 5). On the other hand, there is some evidence that this saturation level depends on the relative importance of convection. The two fully convective M stars fall well below the relationship defined by the other "standard" stars, and even the RS CVn stars tend to fall a little below the main-sequence stars in the saturated regime. The NTTSs are the best indicators of the importance of traditional activity induced emission on CTTSs, and two of the three NTTSs in Figure 5 are also well below the standard star saturation level. All three of the NTTSs in this plot are early-type (older) TTSs which have radiative cores, while the majority of the CTTSs are K7 or later and are fully convective. We do not have activity measurements for a wide enough range of NTTSs to properly constrain the C IV saturation level for all TTSs, but we adopt here a rough saturation limit for surface flux of 10^6 ergs cm^{-2} s^{-1}, indicated by the dash-dotted line in Figure 5. Emission above this saturation level is presumably due to some physical process other than activity. We can convert this surface flux saturation limit to saturated line luminosities for each star, which are then removed from the observed line luminosities to produce *excess* C IV line luminosities. Figure 7 shows these *excess* C IV luminosities versus mass accretion rate, using extinction data from Table 1 as needed. The plot would be qualitatively similar with a bit more scatter, if excess surface flux were plotted, rather than excess luminosity. However, we believe that global luminosity is the relevant quantity when comparing to the global mass accretion rate (as opposed to the accretion rate per unit stellar surface area).

Figure 7 shows a good correlation of the C IV luminosity with mass accretion rate over almost 3 orders of magnitude in mass accretion rate and more than 2 orders of magnitude in C IV luminosity. The linear correlation coefficient for the points in the log-log plot is $r = 0.78$ with an associated FAP of $f_p = 2.6 \times 10^{-3}$. We remind the reader that the optical emission on CTTSs from which the mass accretion rates have been derived is known to be variable and that we see substantial variation in the C IV emission from many CTTSs (Paper I). Therefore, some of the scatter seen in the Figure 7 may be due to the nonsimultaneous nature of the two data sets being compared.

Since there are differences in extinctions and mass-loss rates derived by various previous investigators, it is interesting to explore whether the correlation in Figure 7 depends on the source of these CTTS parameters. In Figure 8 we compare excess C IV luminosity with mass accretion rates from (*a*) Valenti et al. (1993a), (*b*) Hartigan et al. (1995), and (*c*) Gullbring et al. (1998). In each case, we use self-consistent extinctions from each respective study to convert observed line fluxes to excess line luminosities. The overlap

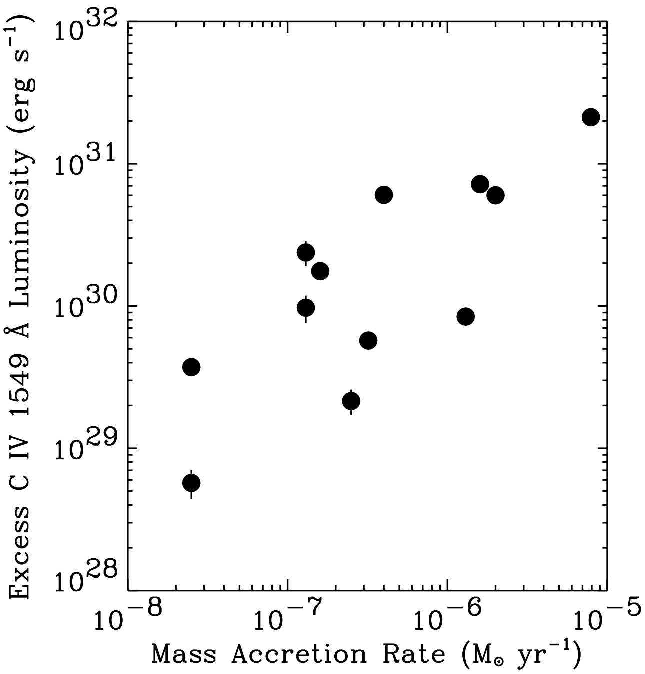

FIG. 7.—*Excess* C IV luminosity vs. the stellar mass accretion rate for several CTTSs in our sample. The accretion rates are from Hartigan et al. (1995).

between each of these investigations and our *IUE* sample is smallest for Gullbring et al. Given with each panel is the correlation coefficient, *r*, and the associated FAP. Obviously, the Hartigan et al. (1995) results produce an excellent correlation. Only one star strays a bit from the relationship defined by the others, and considering the nonsimultaneity of the data sets, this could easily be attributed to intrinsic variability. Only a weak correlation exists with the Valenti et al. (1993a) mass accretion rates, and no correlation at all exists with the Gullbring et al. (1998) mass accretion rates. Since the Hartigan et al. (1995) extinction values are generally the largest of the three studies, one might worry that the excellent correlation in Figure 8*b* is simply the result of applying a range of large corrections to both the optical continuum measured by Hartigan et al. and the UV flux used here. However, Figure 7 shows that the correlation persists, even when using the lower extinction values of Gullbring et al.

The correlations in Figure 7 and 8*b* are so good, it is tempting to use the empirical relationships defined by these figures to estimate mass accretion rates for the remainder of the CTTSs for which we have C IV luminosity measurements. Therefore, we fit a linear relationship between the log of the excess C IV emission and the log of the mass accretion rate. In the first case we use the relationship defined in Figure 7, and in the second case we use that in Figure 8*b*. The relations are

$$\log \dot{M} = 1.318 \log E_{\rm C\,IV} - 46.22 , \quad (1)$$

and

$$\log \dot{M} = 0.753 \log E_{\rm C\,IV} - 29.89 , \quad (2)$$

where $E_{\rm C\,IV}$ is the excess C IV luminosity (in ergs s^{-1}) above an activity saturation level of 10^6 ergs cm^{-2} s^{-1} and $\dot{M}$ is in $M_\odot$ yr^{-1}. The resulting mass accretion rates are reported in Table 4. The two sets of accretion rates thus derived are

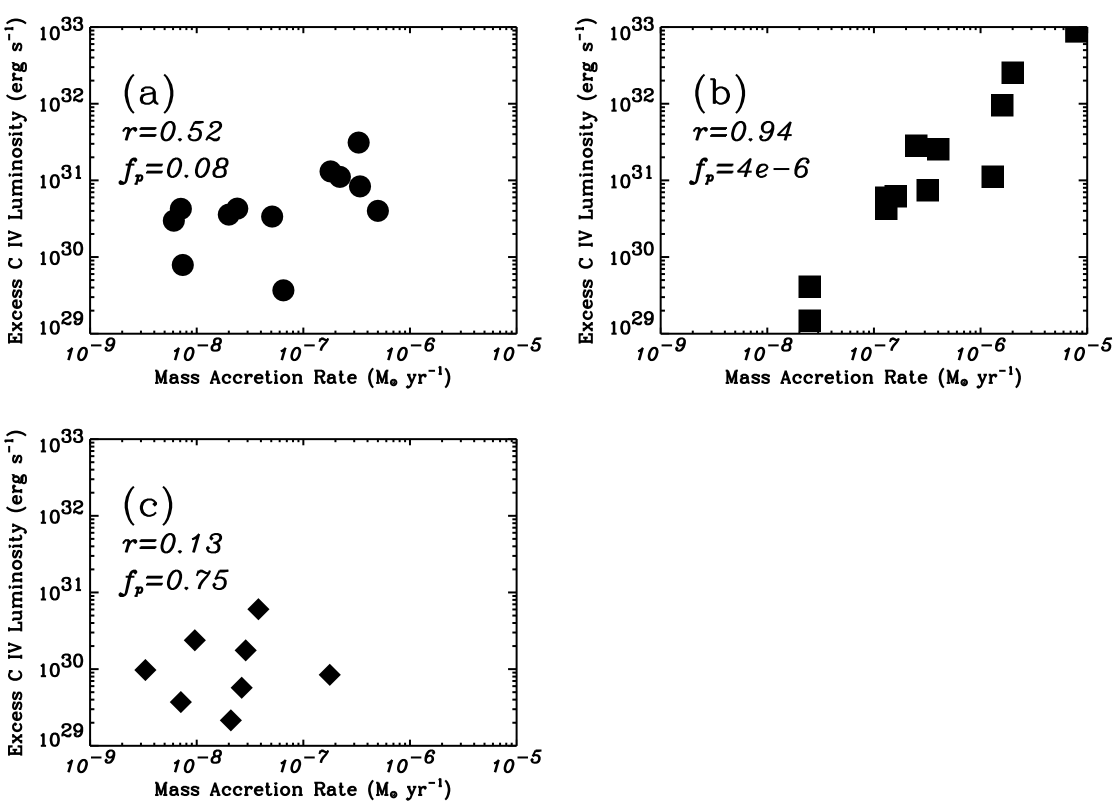

FIG. 8.—*Excess* C IV luminosity plotted vs. mass accretion rate: (*a*) Using Valenti et al. (1993a) mass accretion rates and extinction values; (*b*) using Hartigan et al. (1995) mass accretion rates and extinction values; (*c*) using Gullbring et al. (1998) mass accretion rates and extinction values.

TABLE 4

Mass Accretion Rate Estimates

Index	Star Name	$\dot{M}$[a] ($M_\odot$ yr^{-1})	$\dot{M}$[b] ($M_\odot$ yr^{-1})
13	T Tau	4.8×10^{-6}	3.0×10^{-7}
32	SU Aur	7.6×10^{-7}	1.0×10^{-7}
38	GW Ori	1.8×10^{-5}	6.5×10^{-7}
95	CS Cha	1.7×10^{-6}	1.6×10^{-7}
98	VW Cha	1.3×10^{-4}	2.0×10^{-6}
103......	CV Cha	1.2×10^{-4}	1.9×10^{-6}
113......	RU Lup	2.5×10^{-5}	7.7×10^{-7}
116......	RY Lup	4.2×10^{-8}	2.0×10^{-8}
118......	EX Lup	2.5×10^{-8}	1.5×10^{-8}
120......	HO Lup	2.0×10^{-6}	1.8×10^{-7}
123......	Sz 102	1.4×10^{-6}	1.5×10^{-7}
125......	AS 205	1.9×10^{-5}	6.7×10^{-7}
129......	SR 9	3.5×10^{-7}	6.7×10^{-8}
132......	AS 209	1.0×10^{-6}	1.3×10^{-7}
160......	DI Cep	7.8×10^{-6}	4.0×10^{-7}

[a] Based on eq. (1) derived from the relationship shown in Fig. 7.

[b] Based on eq. (2) derived from the relationship shown in Fig. 8*b*.

extremely well correlated since both are based on Hartigan et al. (1995) mass accretion rates and both begin with the same C IV fluxes. Equation (1) is based primarily on extinctions from Gullbring et al. (1998), but none of the stars in stars in Table 4 have Gullbring et al. extinctions, so values from Table 1 are used instead. The Gullbring et al. extinction values are systematically lower than those in previous studies, giving lower C IV luminosities once a correction is applied. For stars with higher extinctions, the derived excess C IV luminosity can be substantially larger than those used to derive equation (1), leading to unrealistically high estimates of the mass accretion rate as seen in the third column of Table 4. Equation (2) is derived using extinctions from Hartigan et al. (1995) which are generally consistent with other estimates of the extinction, thus the accretion rate estimates in column 4 of Table 4 are similar in range to those in Figure 8*b*. As a result, we favor the calibration given in equation (2) and the associated mass accretion rates in Table 4. On the other hand, since both the accretion rates of Valenti et al. (1993a) and Gullbring et al. (1998) are systematically lower than those of Hartigan et al. by about an order of magnitude, the mass accretion rates in Table 4 may need adjustment down by the same factor.

Table 4 gives mass accretion rates for many stars that have never had their accretion rates measured before. Of particular note are the earlier type CTTSs such as T Tau (K0) and SU Aur (G2), which do not show any optical veiling due to their relatively bright photospheres. For these stars, their FUV emission may be the only means of reliably determining mass accretion rates. The exact relationships derived above depend on placement of the dashed-dotted line in Figure 5. While the dashed line drawn in Figure 5 is defined by the upper envelope of main-sequence stars, the dashed-dotted line is our best guess as to the actual saturation limit for CTTSs. Measurements of NTTSs can be used to define the proper placement for TTSs as a whole; however, there are not enough NTTS measurements, particularly at the later spectral types where the stars are fully convective, to know if this is truly representative of the upper envelope of magnetic activity in TTSs as a whole.

3.5. *Density Estimates*

Figure 1 shows that each emission line observed by *IUE* is well correlated with the others and that line strengths also correlate well with the continuum flux. Therefore, all lines likely have a common emission mechanism (with the possible exception of H_2, as noted above). The correlations shown in Figures 7–9 are similar when constructed for the other lines detected by *IUE*. If most of the *IUE* SWP emission from CTTSs arises in accretion shocks, we can use known density sensitive line ratios to test current accretion shock models and to look for correlations of the density with mass accretion rate. The most recent detailed work on CTTS accretion shocks (Calvet & Gullbring 1998) characterize each model in terms of the energy flux in the accretion column, $F = (1/2)\rho v_s^3$, just before the shock. Calvet & Gullbring (1998) assume a strong shock, so that the postshock density is 4 times the initial density. Thus, simply inverting this equation to give $\rho = n m_{\rm H} \mu = 2(4)F/v_s^3$, we have $n = 8F/(m_{\rm H} \mu v_s^3)$ in the postshock region where μ is the mean molecular weight of the accreting material (taken to be 1.4) and $m_{\rm H}$ is the mass of a hydrogen atom. Calvet & Gullbring (1998) find that $F = 10^{11}$ ergs s^{-1} cm^{-2}, when combined with a canonical mass (0.5 $M_\odot$) and radius (2 $R_\odot$) for CTTSs, yields $v_s = 2.75 \times 10^7$ cm s^{-1}, resulting in a postshock number density of $n = 1.6 \times 10^{13}$ cm^{-3}. The range of parameters required by Calvet & Gullbring (1998) to fit the observed optical excess continua of a dozen or so CTTSs yields postshock densities which vary about this value by less than an order of magnitude. Just after the shock, the material is quite hot ($T \sim 10^6$ K) and cools, becoming more dense in the process. While Calvet & Gullbring are specifically modeling the optical shock emission produced in material substantially more dense than this, the above expression represents the minimum density in the shocked material at any temperature. The density is more than 10^{14} cm^{-1} when the material reaches the temperature of line formation relevant to the *IUE* observations shown here.

The relatively narrow temperature range over which the majority of the lines detected in the *IUE* SWP form allows certain line pairs to be used as density indicators. Cram et al. (1980) first used the C III λ1909–Si III λ1892 and C III λ1909–Si IV λ1403 line pairs to estimate the density in the line emission region of the CTTSs RW Aur and RU Lup, deriving a value of log $n_e = 10.2 \pm 0.6$. Following Cram et al., we use the results of Doscheck et al. (1978b) to derive densities from the C III λ1909–Si III λ1892 line ratio, and we use the results of Doschek et al. (1978a) to derive the density from the C III λ1909–Si IV λ1403 line ratio. The derived densities are reported in Table 5 for all TTSs with the required line measurements.

Such density determinations involve several uncertainties, notably the relative abundances of C and Si and the use of an isothermal model to compute the theoretical relationship between the density and observed line ratio. The above papers assume solar abundance ratios. In the case of an accretion shock, the relevant abundance is that of the incoming disk material which is accreting onto the star. Thus, effects such as the abundance differentiation known to be present in the solar corona relative to the photosphere (the FIP effect) should be unimportant. To our knowledge, no systematic study of the relative abundance of C and Si has been performed for TTSs; however, the ratio would

TABLE 5

DENSITY ESTIMATES

Index	Star	C III λ1909 [a] / Si III λ1892	log n_e (cm^{-3})	C III λ1909 [b] / Si IV λ1403	log n_e (cm^{-3})	C III λ1176 [b] / C III λ1909	log n_e (cm^{-3})
8	V410 Tau	...	...	1.06 ± 0.61	10.4 ± 0.3	...	...
9	BP Tau	0.33 ± 0.04	10.1 ± 0.1	0.31 ± 0.05	11.0 ± 0.1	7.62 ± 1.43	10.3 ± 0.2
10	DE Tau	0.71 ± 0.14	9.7 ± 0.1	1.57 ± 0.84	10.2 ± 0.3	...	...
11	RY Tau	0.67 ± 0.02	9.7 ± 0.1	1.45 ± 0.05	10.3 ± 0.1	...	...
13	T Tau	1.43 ± 0.08	9.3 ± 0.1	1.37 ± 0.19	10.3 ± 0.1	...	...
14	DF Tau	1.69 ± 0.20	8.9 ± 0.2	0.78 ± 0.06	10.6 ± 0.1	...	...
15	DG Tau	1.49 ± 0.29	9.0 ± 0.1	1.81 ± 0.59	10.1 ± 0.2	...	...
18	DK Tau	0.43 ± 0.21	10.0 ± 0.1	0.54 ± 0.38	10.7 ± 0.4	...	...
27	DR Tau	0.72 ± 0.05	9.7 ± 0.1	0.81 ± 0.09	10.6 ± 0.1	...	...
30	LkCa 19	1.72 ± 0.56	8.6 ± 0.2	0.77 ± 0.18	10.6 ± 0.2	...	...
32	SU Aur	0.94 ± 0.04	9.5 ± 0.1	1.36 ± 0.50	10.3 ± 0.2	...	...
38	GW Ori	0.82 ± 0.09	9.6 ± 0.1	0.66 ± 0.11	10.7 ± 0.1	...	...
93	TW Hya	2.17 ± 0.76	< 8.0	...	...	...	...
103	CV Cha	0.27 ± 0.04	10.2 ± 0.1	0.48 ± 0.12	10.8 ± 0.1	...	...
113	RU Lup	0.42 ± 0.02	10.0 ± 0.1	0.50 ± 0.04	10.8 ± 0.1	5.05 ± 0.43	10.0 ± 0.1
118	EX Lup	0.28 ± 0.05	10.2 ± 0.1	0.32 ± 0.05	11.0 ± 0.1	...	...
123	Sz 102	1.39 ± 0.19	9.0 ± 0.1	1.14 ± 0.29	10.4 ± 0.2	...	...
133	AK Sco	0.57 ± 0.03	9.8 ± 0.1	...	...	...	...
143	AS 292	...	...	...	...	...	...
144	FK Ser A	0.91 ± 0.16	9.5 ± 0.1	...	...	...	...
160	DI Cep	0.43 ± 0.04	10.0 ± 0.1	0.57 ± 0.06	10.7 ± 0.1	...	...

[a] Flux ratio not corrected for extinction since the effect is negligible over the small wavelength interval.
[b] Flux ratio is corrected for extinction. If no extinction estimate is available, no value is given.

have to be a factor of 100–1000 different from the solar ratio to bring the observations into agreement with the shock calculations of Calvet & Gullbring (1998).

One way to remove the ambiguity of an unknown relative abundance is to use lines from the same element. Cook & Nicolas (1979) show that C III λ1176–C III λ1909 can be used as a density sensitive line measure of solar transition region material. Unfortunately, the C III λ1176 line is in a poor region for *IUE*. In most spectra, this part of the spectrum is dominated by noise, and the line is not distinguishable. Only in four CTTSs (particularly bright or with many observations to improve the S/N) is this line apparent in the atlas of Paper I; however, only for two of these do we have an estimate of the extinction which is required to use these two lines which are widely separated in wavelength. For these two stars we have measured the flux in the C III line and used the relationships given in Cook & Nicolas (1979) to determine the density (using the $T = 5.6 \times 10^4$ K curve of their Figure 5, corresponding to the temperature of peak emissivity for these lines). The resulting densities are also given in Table 5. These two estimates are similar to the results for the other line ratios for each given star, indicating that uncertainties in the relative abundance of C and Si is not a major problem.

The other major uncertainty in using line ratios to estimate density is the assumption of an isothermal source when computing the relationship between these two quantities. Cook & Nicolas (1979) explored these effects for the C III λ1176–C III λ1909 line ratio by computing isothermal models at $T_e = 3 \times 10^4$ K and $T_e = 1.26 \times 10^5$ K, where the emissivity in these lines is down by factors of 3–100 relative to the $T_e = 5.6 \times 10^4$ K model. The resulting estimates of the line ratio as a function of density implies densities different from their default determination by 0.5 dex. Since real shock models will have emission measure at all these temperatures, these differences are a bit of an overestimate. Nevertheless, we adopt a systematic uncertainty of 0.5 dex in the density estimate from the C III λ1176–C III λ1909 line ratio. Unfortunately, Doschek et al. (1978a, 1978b) do not perform a similar analysis for the other line ratios used above. Therefore, we have used the CHIANTI atomic database and associated coronal equilibrium code (Landi et al. 1999; Dere et al. 1997) to calculate the dependence of these line ratios on density at several temperatures between $T_e = 3 \times 10^4$ K and $T_e = 1.26 \times 10^5$ K. At these extremes, the emissivity in both the C III λ1909 and the Si IV λ1403 lines is down by more than an order of magnitude from its peak at $T_e \sim 7 \times 10^4$ K. Throughout this temperature range, there is a full spread of 0.6 dex in the derived density for a given C III λ1909–Si IV λ1403 line ratio for densities $\sim 10^{10}$ cm^{-3}. Therefore, we estimate a total uncertainty of about ±0.5 dex in the derived densities based on individual line ratios from the *IUE* SWP spectra.

Using density sensitive line ratios in the *IUE* spectra of CTTSs, we find typical densities of log n_e = 9.0–11.0. The current shock models of Calvet & Gullbring (1998) require log n_e = 13–14. It is doubtful that systematic effects due to nonsolar abundance patterns or uncertainties in the temperature distribution can account for these differences. On the other hand, Gómez de Castro & Lamzin (1999) have made a different set of shock calculations and find that their accretion shocks can reproduce the emissions observed by *IUE* in a handful of CTTSs if the density is in the range 10^{10}–10^{11}, as found in Table 5. Thus, it appears that accretion shocks are a viable source for the emission lines seen in the *IUE* SWP provided the densities are not too high.

On the other hand, it must be kept in mind that there is probably also emission from a standard stellar transition region in these CTTSs, an effect not considered by Calvet & Gullbring or Gómez de Castro & Lamzin. Such stellar transition regions have a typical density of log n_e = 9.3–10.3 (Doschek et al. 1978b), similar to many of the densities found in Table 5. Sufficient emission from a stellar transition region on a CTTS would dilute the line ratio produced by a denser accretion shock region, resulting in a lower derived density for the accretion shock. Assuming the accretion shock is at a density of log $n_e = 13.0$, and its emission is being diluted by a transition region with a density of log $n_e = 10.0$, we use the C III λ1909–Si IV λ1403 line ratio calculation of Doschek et al. (1978a) to estimate the relative contribution of these two components which gives a final line ratio indicative of log $n_e = 11.0$. The resulting ratio of transition region emission to accretion shock emission in the C III λ1909 line is more than 900 in this case, implying that the C III line is not indicative of the accretion shock at all. If this is indeed the case, we expect the C III λ1909 emission of CTTSs to be similar to other active stars. In Figure 9 we show the C III λ1909 surface flux plotted against $\tau_c/P_{\rm rot}$. This figure is similar to Figure 5 for C IV, but here the C III emission from the CTTSs is about an order of magnitude stronger on average than from main-sequence stars of similar Rossby number. Thus, it is more likely that the C III emission is indeed produced in the accretion shock, and the density in this shock is log $n_e = 10.0$–11.0 with a correspondingly larger surface area covering fraction.

We next looked for correlations of the density and temperature of the shocked gas with the mass accretion rate. Since Figure 1 shows that all the lines and continua are well correlated, and Figures 7, 8*b*, and 9 indicate that the line luminosity is a good proxy for the mass accretion rate, we looked for correlations of the two density sensitive line ratios given in Table 5 with the C III luminosity. No correlation was evident. As a temperature indicator, we take the ratio of the two continuum values and compare that to the 1958 Å continuum luminosity. Since Figure 3 shows that the stellar continuum becomes important at higher effective temperatures, we restrict this comparison to those CTTSs

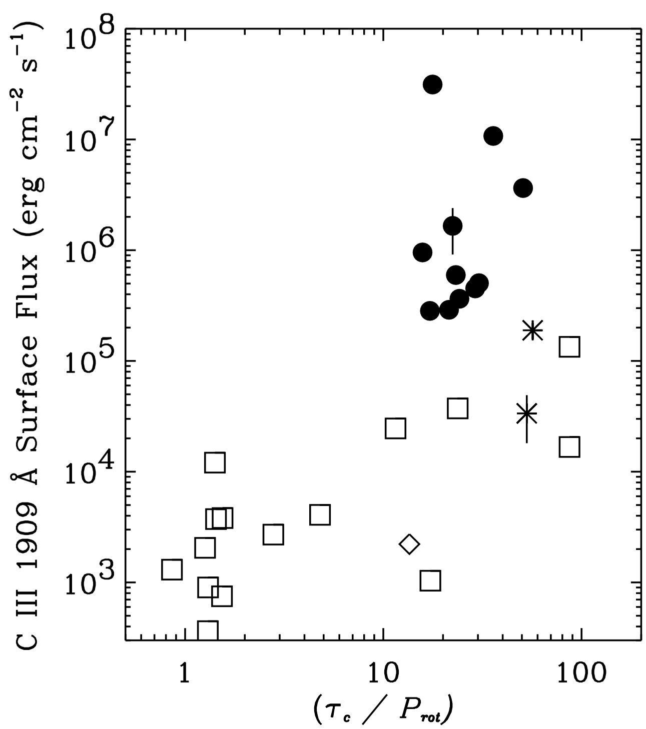

FIG. 9.—C III 1909 Å surface flux vs. $\tau_c/P_{\rm rot}$ (proportional to the dynamo number). The plot symbols are the same as those of Fig. 4.

with $T_{\rm eff} \leq 4400$ K. Again, no correlation was found, indicating the shock temperature is also independent of the mass accretion rate.

Finally, we looked for correlations of any of the *IUE* emission surface fluxes or luminosities with the IR excess ($\Delta H - K$) and found none, even when comparing molecular hydrogen emission properties with the IR excess. This makes sense in terms of the UV fluorescent excitation method for H_2: the primary limitation to the molecular hydrogen emission is the number of UV pump photons available, not the vast amounts of H_2 that might be present.

4. SUMMARY AND DISCUSSION

We have analyzed the continuum and emission lines present in the *IUE* short-wavelength bandpass for the TTSs in the pre–main-sequence *IUE* atlas of Paper I. We find that all detected lines and the continuum in the 1250–2000 Å range are well correlated with each other. At first sight it is surprising that the molecular hydrogen lines are well correlated with the other lines, since the H_2 lines probe material at a temperature of $\sim$2000 K, while the other lines detected by *IUE* trace material at a temperature close to $\sim 10^5$ K. On further consideration, the H_2 lines are pumped by UV emission from Lyα (Paper I), so such a correlation should be expected.

It is clear that the cooler CTTSs have UV continuum surface flux emission levels that are substantially stronger than the most magnetically active main-sequence stars of similar spectral type. This continuum emission appears to be the short-wavelength extension of the blue excess emission seen in the optical, which has been interpreted in terms of accretion luminosity (Hartigan et al. 1991; Valenti et al. 1993a; Hartigan et al. 1995; Gullbring et al. 1998). In fact, using the simple boundary layer model of Valenti et al. (1993a) to compute the continuum emission in the SWP bandpass gives flux levels typically within a factor of 2 of the level observed. As mentioned before, uncertainties in the extinction to CTTSs can easily account for such differences, not to mention the intrinsic variability of these stars. The warmer CTTSs and the NTTSs (also generally warmer) appear to have an increasing contribution from the underlying magnetically heated stellar photosphere, making clear extraction of the accretion component difficult.

We then explored the hypothesis that the "transition region" line emission from TTSs seen by *IUE* is the result of dynamo-generated magnetic activity. Comparing the emission level in TTSs with main-sequence and RS CVn magnetic "standard" stars, we showed that the few NTTSs observed by *IUE* do seem to fit into this general magnetic paradigm, but that the CTTSs do not. The CTTSs appear to have excess line emission compared to the main-sequence and RS CVn "standards" and to the NTTSs. Since the CTTSs are the only stars of these groups that are currently undergoing accretion, excess line emission from the accretion shocks appears to be a natural explanation for their anomalous line strength. We then empirically explored the relationship between C IV line luminosity and mass accretion rate in CTTSs, finding some evidence for the existence of a correlation. Comparing the C IV line emission with the mass accretion rates determined by Hartigan et al. (1995) shows an excellent correlation, independent of the exact extinction values to calculate the C IV emission. Comparing the line luminosity with the mass accretion rates derived by Valenti et al. (1993a) shows a weak correlation, and using the mass accretion rates derived by Gullbring et al. (1998) shows no correlation with line emission properties. This is surprising since Gullbring et al. (1998) show that their derived accretion luminosity is well correlated with those determined by both Valenti et al. (1993a) and Hartigan et al. (1995). The overlap of the Gullbring et al. sample with that observed by *IUE* happens to be the smallest of these three papers, and perhaps the intrinsic variability of CTTSs combined with this small sample conspired to produce no correlation. On the other hand, the lack of correlation between the C IV line and the accretion rates of Valenti et al. and Gullbring et al. is a concern for the accretion origin of the $T = 10^5$ K emission lines observed by *IUE* in CTTSs.

Operating under the assumption that the line emission from CTTSs does arise from the accretion shock, line ratios were used to determine the density of $\sim 10^5$ K material in the postshock region, which were compared to recent models by Calvet & Gullbring (1998). The models appear to overpredict the density by 3–4 orders of magnitude. The models could be brought into better agreement with these observations if the density in the accreting material is lowered, which will require a corresponding increase in the accretion shock filling factors to maintain the same mass accretion rates. Accretion filling factors have been published for sizeable samples of CTTSs by Calvet & Gullbring (1998) and by Valenti et al. (1993a). Comparing derived values of the filling factor for stars in common between these two studies shows that Calvet & Gullbring values are on average lower than those of Valenti et al., but by only a factor of ~ 3 with considerable scatter about this average. Such a small difference does not explain the sizeable discrepancy in the density. The difference might be accounted for by more serious adjustment of the accretion shock models. For example, lowering the velocity of the infalling material so that its immediate postshock temperature and density are substantially lower could substantially lower the density of this material by the time it has cooled to the $\sim 7 \times 10^4$ K temperature indicative of the emission lines seen by *IUE*. This change, combined with an increase in the filling factor, may bring the predicted densities into better agreement with the observations presented here, though this may have strong negative effects on the predicted optical emission these models were developed to explain. Nevertheless, inclusion of "transition region" line emission as traced by *IUE* provides a strong additional constraint on the structure of the magnetically controlled accretion shocks on CTTSs.

Finally, we looked for a correlation of the density or temperature in the accretion shock with mass accretion rate but found none. This suggests that the primary difference between CTTSs with different mass accretion rates is the surface area of the star covered by the accretion shock, a result previously found by Valenti et al. (1993a) and Gullbring et al. (1998). It should be reemphasized, however, that the association of far-UV emission from CTTSs with accretion shocks is strong but not yet conclusive. The latest accretion rate measurements by Gullbring et al. (1998) do not show any correlation with *IUE* emission strength. Matching high-resolution line profiles of the high-temperature lines will provide an additional test of the hypothesis that accretion-related processes are a dominant contributor to the high-temperature emission lines seen in CTTSs (e.g., Gómez de Castro, Lamzin, & Shatskii 1994; Calvet et al. 1996).

The fully convective nature of TTSs may make the dynamo operating in these stars very different from that in the main-sequence and RS CVn comparison stars we have considered here. The NTTSs are the most appropriate proxies for the stellar activity present on CTTSs, but very few NTTSs were observed with *IUE*. Additional observations of NTTSs, perhaps with the STIS instrument onboard *HST*, are needed to verify that the emissions seen from CTTSs are in fact statistically in excess of what is produced by the magnetically active central star. Such an observation will solidify the need for an additional energy source to produce the observed emission, with accretion the most appropriate candidate.

We would like to thank the referee, Gibor Basri, for his careful reading of the original manuscript and the many useful comments relayed to us. We would also like to thank NASA for support through grant S-56500-D to the University of Colorado. C. M. J. would also like to acknowledge partial support from NASA grant NAG5-8209 to the University of California. The work reported in this paper made extensive use of the SIMBAD database maintained by the Centre de Données Astronomiques de Strassbourg.

REFERENCES

Appenzeller, I., Jankovics, I., & Krautter, J. 1983, A&AS, 53, 291
Baliunas, S. L., et al. 1995, ApJ, 438, 269
Barry, D., Hege, K., & Cromwell, R. H. 1984, ApJ, 277, L65
Basri, G. 1987, ApJ, 316, 377
Basri, G., & Batalha, C. 1990, ApJ, 363, 654
Basri, G., & Bertout, C. 1989, ApJ, 341, 340
———. 1993, in Protostars & Planets III, ed. E. H. Levy & J. I. Lunine (Tucson: Univ. Arizona), 543
Basri, G., Laurent, R., & Walter, F. M. 1985, ApJ, 298, 761
Bertout, C. 1989, ARA&A, 27, 351
Bertout, C., Basri, G., & Bouvier, J. 1988, ApJ, 330, 350
Bessell, M. S., & Brett, J. M. 1988, PASP, 100, 1134
Bevington, P. R., & Robinson, D. K. 1992, Data Reduction and Error Analysis for the Physical Sciences (New York: McGraw-Hill)
Brown, A., de M. Ferraz, M. C., & Jordan, C. 1984, MNRAS, 207, 831
Bouvier, J. 1990, AJ, 99, 946
Bouvier, J., & Bertout, C. 1989, A&A, 211, 99
Bouvier, J., Bertout, C., & Bouchet, P. 1986, A&A, 158, 149
Bouvier, J., Cabrit, S., Fenandez, M., Martin, E. L., & Matthews, J. M. 1993, A&A, 272, 176
Bouvier, J., Covino, E., Kovo, O., Martín, E. L., Matthews, J. M., Terranegra, L., & Beck, S. C. 1995, A&A, 299, 89
Cabrit, S., Edwards, S., Strom, S. E., & Strom, K. M. 1990, ApJ, 354, 687
Calvet, N., Basri, G., & Kuhi, L. V. 1984, ApJ, 277, 725
Calvet, N., & Gullbring, E. 1998, ApJ, 509, 802
Calvet, N., Hartmann, L., Hewett, R., Valenti, J., Basri, G., & Walter, F. 1996, in ASP Conf. Ser. 109, Cool Stars, Stellar Systems, and the Sun, Ninth Cambridge Workshop, ed. R. Pallavicini & A. K. Dupree (San Francisco: ASP), 419
Camenzind, M. 1990, Rev. Mod. Astron., 3, 234
Cohen, M., & Kuhi, L. V. 1979, ApJS, 41, 743
Cook, J. W., Brueckner, G. E., & Bartoe, J.-D. 1983, ApJ, 270, L89
Cook, J. W., & Nicolas, K. R. 1979, ApJ, 229, 1163
Cram, L. E. 1979, ApJ, 234, 949
Cram, L. E., Giampapa, M. S., & Imhoff, C. L. 1980, ApJ, 238, 905
D'Antona, F., & Mazzitelli, I. 1994, ApJS, 90, 467
Dere, K. P., Landi, E., Mason, H. E., Monsignori Fosi, B. C., & Young, P. R. 1997, A&AS, 125, 149
Doschek, G. A., Feldman, U., Bhatia, A. K., & Mason, H. E. 1978a, ApJ, 226, 1129
Doschek, G. A., Feldman, U., Mariska, J. T., & Linsky, J. L. 1978b, ApJ, 226, L35
Duncan, D. K., et al. 1991, ApJS, 76, 383
Durney, B. R., De Young, D. S., & Roxburgh, I. W. 1993, Sol. Phys., 145, 207
Durney, B. R., & Latour, J. 1978, Geophys. Astrophys. Fluid Dyn., 9, 241
Feldman, U., & Doschek, G. A. 1978, ApJS, 37, 443
Gauvin, L. S., & Strom, K. M. 1992, ApJ, 385, 217

Ghez, A. M., Neugebauer, G., & Matthews, K. 1993, AJ, 10, 2005
Giampapa, M. S., Calvet, N., Imhoff, C. L., & Kuhi, L. V. 1981, ApJ, 251, 113
Gilliland, R. G. 1985, ApJ, 299, 286
———. 1986, ApJ, 300, 339
Gómez de Castro, A. I., & Fernández, M. 1996, MNRAS, 283, 55
Gómez de Castro, A. I., & Franqueira, M. 1997, ApJ, 482, 465
Gómez de Castro, A. I., & Lamzin, S. A. 1999, MNRAS, 304, L41
Gómez de Castro, A. I., Lamzin, S. A., & Shatskii, N. I. 1994, Astron. Rep., 38, 540
Gray, D. F. 1992, The Observation and Analysis of Stellar Photospheres (New York: Cambridge Univ. Press)
Green, T. P., & Young, E. T. 1992, ApJ, 395, 516
Gullbring, E., Hartmann, L., Brice, C., & Calvet, N. 1998, ApJ, 492, 323
Haisch, B. M., & Basri, G. 1985, ApJS, 58, 179
Hamann, F., & Persson, S. E. 1992, ApJ, 394, 628
Hartigan, P., Kenyon, S. J., Hartmann, L., Strom, S. E., Edwards, S., Welty, A. D., & Stauffer, J. 1991, ApJ, 382, 617
Hartigan, P., Edwards, S., & Ghandour, L. 1995, ApJ, 452, 736
Hartmann, L., Hewett, R., Stahler, S., & Mathieu, R. D. 1986, ApJ, 309, 275
Hartmann, L. W., & Kenyon, S. J. 1990, ApJ, 349, 190
Hartmann, L., Soderblom, D. R., Noyes, R. W., Burnham, N., & Vaughan, A. H. 1984, ApJ, 276, 254
Henry, T. J., Soderblom, D. R., Donahue, R. A., & Baliunas, S. L. 1996, AJ, 111, 439
Herbig, G. H. 1962, Adv. Astron. Astrophys., 1, 47
———. 1970, Mem. R. Soc. Sci. Liége (5), 9, 13
Herbig, G. H., & Bell, K. R. 1988, Lick Obs. Bull. 1111
Herbig, G. H., & Goodrich, W. 1986, ApJ, 309, 294
Herbig, G. H., & Soderblom, D. R. 1980, ApJ, 242, 628
Herbst, W., et al. 1987, AJ, 94, 137
Hughes, J., Hartigan, P., Krautter, J., & Kelemen, J. 1994, AJ, 108, 1071
Imhoff, C. L., & Appenzeller, I. 1987, Scientific Accomp. of the *IUE*, ed. Y. Kondo (Dordrecht: Reidel), 295
Johns-Krull, C. M. 1996, A&A, 306, 803
Johns-Krull, C. M., & Valenti, J. A. 2000, in ASP Conf. Ser., Stellar Clusters and Associations: Convection, Rotation, and Dynamos, ed. R. Pallavicini, G. Micela, & S. Sciotino (San Francisco: ASP), 371
Johns-Krull, C. M., Valenti, J. A., & Koresko, C. 1999, ApJ, 516, 900
Judge, P. G., & Carpenter, K. G. 1998, ApJ, 494, 828
Kim, Y.-C., & DeMarque, P. 1996, ApJ, 457, 340
Königl, A. 1991, ApJ, 370, L39
Lamzin, S. A. 1995, A&A, 295, L20
Lamzin, S. A. 1998, Astron. Rep., 42, 322
Landi, E., Landini, M., Dere, K. P., Young, P. R., & Mason, H. E. 1999, A&AS, 135, 339
Lawson, W. A., Feigelson, E. D., Huenemoerder, D. P. 1996, MNRAS, 280, 1071
Liu, M. C., et al. 1996, ApJ, 461, 334
Lynden-Bell, D., & Pringle, J. E. 1974, MNRAS, 168, 603
Nichols, J. S., & Linsky, J. L. 1996, AJ, 111, 517
Noyes, R. W., Hartmann, L. W., Baliunas, S. L., Duncan, D. K., & Vaughan, A. H. 1984, ApJ, 279, 763
Ostriker, E. C., & Shu, F. H. 1995, ApJ, 447, 813
Padgett, D. L. 1996, ApJ, 471, 847
Paatz, G., & Camenzind, M. 1996, A&A, 308, 77
Reipurth, B., Pedrosa, A., & Lago, M. T. V. T. 1996, A&AS, 120, 229
Rutten, R. G. M., Schrijver, C. J., Lemmens, A. F. P., & Zwaan, C. 1991, A&A, 252, 203
Schrijver, C. J. 1987, A&A, 172, 111
Shu, F. H., Najita, J., Ostriker, E., Wilkin, F., Ruden, S., & Lizano, S. 1994, ApJ, 429, 781
Simon, T., Herbig, G., & Boesgaard, A. M. 1985, ApJ, 293, 551
Simon, T., Vrba, F. J., & Herbst, W. 1990, AJ, 100, 1957
Skinner, S. L., Brown, A., & Walter, F. M. 1991, AJ, 102, 1742
Stepień, K. 1994, A&A, 292, 191
Strom, K. M., Strom, S. E., Edwards, S., Cabrit, S., & Skrutskie, M. F. 1989, AJ, 97, 1451
Uchida, Y., & Shibata, K. 1984, PASJ, 36, 105
Valenti, J. A., Basri, G., & Johns, C. M. 1993a, AJ, 10, 2024
Valenti, J. A., Basri, G., Walter, F., Hartmann, L., & Calvet, N. 1993b, BAAS, 183, 40.07
Valenti, J. A., Johns-Krull, C. M., & Linsky, J. L. 2000, ApJS, in press (Paper I)
Vernazza, J. E., Avrett, E. H., & Loeser, R. 1981, ApJS, 45, 635
Vilhu, O. 1984, A&A, 133, 117
Walter, F. M. 1986, ApJ, 306, 573
———. 1987, PASP, 99, 31
Walter, F. M., Brown, A., Mathieu, R. D., Myers, P. C., & Vrba, F. J. 1988, AJ, 96, 297
Walter, F. M., & Byrne, P. B. 1998, ASP Conf. Ser. 154, Cool Stars, Stellar Systems, and the Sun, 10th Cambridge Workshop, ed. R. A. Donahue & J. A. Bookbinder (San Francisco: ASP), 1458
Walter, F. M., Vrba, F. J., Mathieu, R. D., Brown, A., & Myers, P. C. 1994, AJ, 107, 692